JAMES COOK CYCLONE STRUCTURAL TESTING STATION

CYCLONE TESTING STATION

STATIC BEHAVIOUR OF CORRUGATED ROOFING UNDER SIMULATED WIND LOADING

TECHNICAL REPORT No. 33

October 1988

CYCLONE TESTING STATION

STATIC BEHAVIOUR OF CORRUGATED ROOFING UNDER SIMULATED WIND LOADING

M. MAHENDRAN

TECHNICAL REPORT No. 33

October 1988

TABLE OF CONTENTS

ABSTRACT

As a first step to study the fatigue behaviour of light gauge corrugated steel roofing under cyclic uplift wind loading, experimental and finite element analyses of a number of two-span roofing assemblies with different spans and fastening systems were conducted under static loading conditions.

Some interesting, but anomalous observations were noted for crest fastening the alternate corrugations which is the most common fastening system in cyclone prone areas. During the initial stages of loading, significant cross-sectional distortion of the roofing occurred in the case of shorter spans due to greater upward deflections of unscrewed corrugations compared with that of adjoining screwed corrugations. At a load in the range of 550 to 650 Newtons per fastener, a local plastic failure associated with buckling occurred in the vicinity of the central support fasteners for all the spans. This anomalous observation was reported and investigated. However, there was considerable reserve static strength beyond this local failure, particularly for shorter spans. Despite this, the presence of large stresses in the vicinity of central support fasteners indicated that low cycle fatigue cracking could occur in this case. The overall behaviour of roofing fastened at alternate crests with cyclone washers was somewhat similar to that of roofing without washers, but with an increased local plastic failure load for all the spans, the greater increase being for the shorter span.

When alternate corrugations were fastened at the valleys or every corrugation was fastened at the crests, the roofing behaved in a totally different manner and no anomalous behaviour was observed in either case. In the former case, a local plastic failure did not occur despite significant cross-sectional distortion of the roofing, and in the latter case, hardly any cross-sectional distortion of the roofing occurred until the ultimate failure.

Experimental and finite element analytical results agreed reasonably well. These results revealed that the static behaviour of corrugated roofing under uplift wind loading was very much dependent on how the corrugations were fastened. Simple engineering formulae were incapable of predicting the deflections and stresses in the roofing in most cases. The static results have been used to explain the fatigue behaviour of corrugated roofing.

1. INTRODUCTION

Light gauge metal cladding is the most common roofing material in the tropical cyclone prone areas of Australia. The laboratory and field investigations following major cyclones have established the fact that light gauge metal roofing can suffer extensive damage due to fatigue failure in the vicinity of its fasteners (Beck and Morgan, 1975, Morgan and Beck, 1977, Beck and Stevens, 1979). This premature failure of roofing can lead to the failure of other structural elements in the house due to overloading and instability, and eventually to the collapse of the house. During cyclone Tracy which hit the city of Darwin in 1974, 50 to 60 per cent of the traditional timber houses were damaged beyond repair, and over 90 per cent of houses and 70 per cent of all other structures suffered considerable damage to roofing (Walker, 1975).

At present, roofing assemblies for cyclone prone areas are subjected to standard fatigue tests described in TR440 (EBS, 1978) and DABM (DRC, 1976), and the performance of such roofing has improved as evident during recent cyclones (Reardon et al., 1986). However, these performance tests are only providing an approximate answer to the complicated low cycle fatigue problem under rapidly fluctuating cyclonic winds. There have been instances when the roofing systems which passed these tests did not appear to be very much different to those which failed during cyclone Tracy. The fact that two different fatigue tests are being used to assess the fatigue strength of the roofing assemblies within the same cyclonic region of Australia reflects the doubts that prevail regarding these fatigue tests.

Further it is to be noted that the section properties of light gauge metal roofing profiles and the strength properties of sheet material have changed significantly towards high strength and thinner roofing in recent times. Although light gauge metal roofing profiles have been in use for a long time, their use has been mainly based on some limited static and fatigue test results. Hence the Cyclone Testing Station is currently conducting analytical and experimental investigations into the behaviour of light gauge metal roofing with emphasis on corrugated roofing which is the most common roofing profile in the cyclone prone areas of Australia.

As a first step, corrugated roofing assemblies with different spans and fastening systems were considered analytically and experimentally under static uplift wind loading conditions. Attempts were then made to explain the fatigue behaviour of such roofing assemblies based on the static results obtained. This report presents the details of the analytical and experimental methods and the results.

2. EXPERIMENTAL METHOD

2.1 General

Roof claddings are predominantly subjected to uplift wind loading which is due to the combination of external and internal wind pressures. Ideally an investigation on roof claddings should be carried out on full scale multi-span roofing assemblies subjected to realistic wind pressure loading. However, due to practical considerations, a two-span roofing assembly with simply supported ends subjected to midspan line loads was considered adequate to model the critical regions of a multi-span roofing assembly.

The end spans of a roof cladding are generally subjected to greater suction forces during cyclonic winds. The analysis of a multi-span roofing assembly indicates that the second support from the eaves is very often critically loaded when subjected to wind pressure loading. Hence a two-span roofing assembly with simply supported ends representing an end span was chosen to model the critical second support conditions.

Midspan line loading was chosen due to practical limitations associated with the use of a commercial hydraulic testing machine. As uniform pressure loading was not used, it was necessary that the main loading parameters at the critical central support, namely the load per fastener and the bending moment were modelled correctly. Hence a number of equivalent test spans of 250 (short span), 500, 650 (medium spans) and 1000 mm (long span) were selected in order to include a wide spectrum of recommended spans of corrugated roofing. These laboratory test spans are equivalent to prototype end spans of approximately 350, 700, 900 and 1400 mm, respectively, which are subjected to uniform pressure loading. In the following sections of this report, only the laboratory test span values are mentioned.

A different testing method with uniform pressure loading was used for a limited number of tests on two-span roofing assemblies of other spans and on another roofing profile. Brief details of these tests are given in Sections 4.5 and 4.6. All other sections deal only with the main series of tests on corrugated roofing under midspan line loading.

2.2 Test Specimen

Most of the tests were conducted on Lysaght Building Industries' Custom Orb corrugated steel roofing of 0.42 mm base metal thickness (bmt) and 0.47 mm total coated thickness (tct). The corrugated roofing is roll-

formed according to AS 1445 (SAA, 1977) from a Zincalume-coated high tensile steel sheet which complies with grade G550 - AZ150 in AS 1397 (SAA, 1984) (i.e., minimum yield stress of 550 MPa and minimum coating mass of 150 g/m^2). The basic dimensions of the corrugated roofing profile are shown in Figure 1.

Figure 1. Basic Dimensions of Corrugated Roofing Profile

Test specimens were fastened using four different fastening systems, namely alternate crest fastening with or without cyclone washers, every crest fastening without cyclone washers and alternate valley fastening (see Figure 2). The manufacturers of corrugated roofing recommend alternate crest fastening with or without cyclone washers for the use in cyclonic areas, except in the Northern Territory where cyclone washers must be used (LBI, 1987). Alternate crest fastening is referred to as a fixing arrangement with five fasteners per sheet in their reference manual. Every crest fastening is not recommended at all, but alternate valley fastening is recommended for walls. In this investigation, the fastening systems other than those recommended were also used in order to study the dependence of the behaviour of corrugated roofing on such fastening systems.

Due to physical constraints of the testing machine, the specimens in most cases were only six corrugations wide (see Figure 2). It is assumed that the absence of lateral continuity of roofing would have caused very little effect on the overall test results. All the test specimens fastened at alternate crests had three fasteners, but in the case of 650 mm span, four fasteners were also used. Five fasteners were used when the specimen was fastened at every crest. An overhang of 50 mm was provided on either side of the end supports of the roofing assembly for all the spans. In most cases, the roof sheeting was secured to timber battens with no.14 x 50 mm Type 17 hexagonal head self drilling screws with EPDM seals as

recommended by LBI (1987). Shorter screws (25 mm) were used in the case of valley fastening. High quality timber was used in all the tests to prevent premature screw withdrawal from timber. All screws were tightened until the neoprene washers were just prevented from rotating to avoid either overtightened or loose screws. Attempts were made to ensure that all the screws were located exactly at the centre of the crest or valley, and perpendicular to the plane of roofing.

Figure 2. Test Specimens with Different Fastening Systems

2.3 Test Set-up

All tests were conducted on a servo-controlled hydraulic testing machine (Instron) of 200 kN static capacity at the James Cook University Structures Laboratory. Figure 3 shows the test set-up.

CS : Central Support (supported by portal frame above)

SSE : Simply Supported Ends (supported by channel beams)

(a). Line Diagram illustrating the Test Set-up

(b). Overall View of the Test Set-up for Long Span Roofing

Figure 3. Test Set-up

A small portal frame supported the central batten against the load cell above it and thus enabled the average load per fastener at the central support to be monitored directly (see later in Figure 5 (a)). Extreme care was taken to ensure that the line loading system applied pressure uniformly to the underside of the corrugations in both their normal and distorted profiles at each midspan. For this purpose a thin rubber tube filled with water was used on top of a rubber pad of width 30 mm that was moulded in the shape of the roofing profile (see Figure 4).

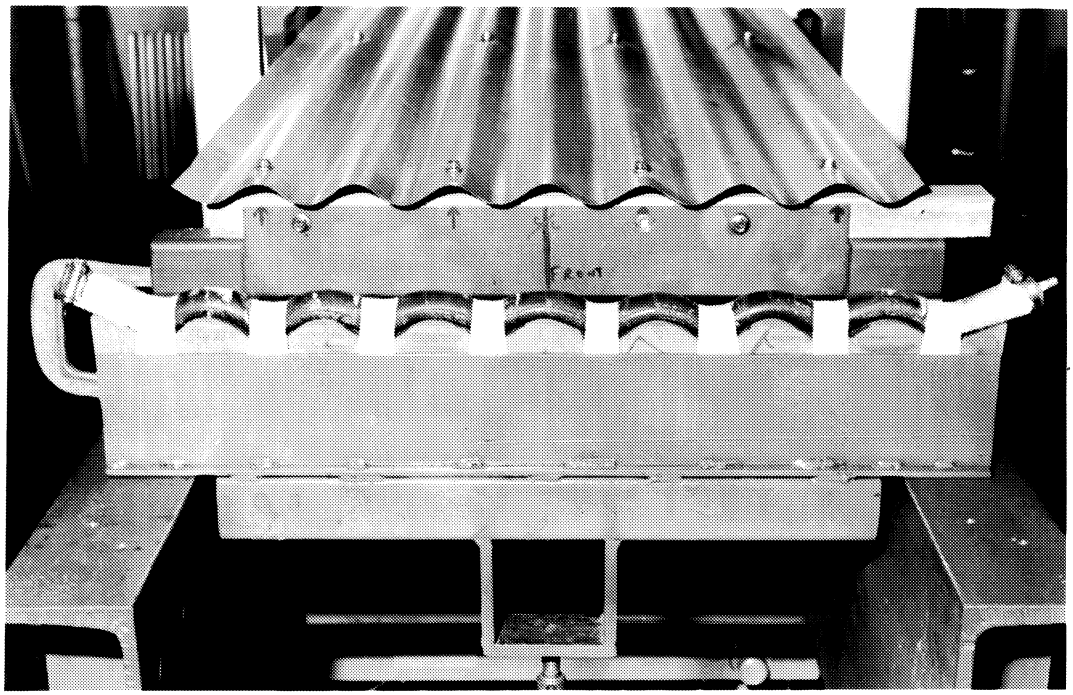

Figure 4. Midspan Line Loading Method

2.4 Testing Method

All tests were conducted by controlling displacement rather than force in order to follow the entire loading path through any unstable localized failure stages. The total reaction force at the central support was directly read from Instron's load display unit. The average load per fastener was thus obtained by dividing the total reaction force by the number of fasteners at the support. Upward deflections of the corrugations normal to the roofing at each midspan and the central support were measured using dial gauges graduated to 0.01 mm. These measurements were taken at suitable intervals depending on the estimated ultimate failure load. Tests were discontinued when the roofing developed global plastic mechanisms across its entire width at sufficient number of locations for the collapse to occur.

2.5 Tests on Strain Gauged Specimens

In order to accurately determine the stresses in the roofing, especially in the vicinity of central support fasteners, two tests were conducted on strain gauged specimens of 250 and 1000 mm spans crest-fastened at alternate corrugations. Strain gauges were positioned at the screwed and unscrewed crests, and the valley between those crests, of both midspan and central support (see Figure 5 (a)). The principal stress directions of the stress field around the central support fasteners were not known beforehand and thus three arm 45 degree strain gauge rosettes were used at four locations around the middle fastener (Figure 5 (b)). These rosettes were located on the crests and sides of corrugations approximately 12 mm from the centre of fastener hole. On locations such as the crests and valleys of the midspan and the unscrewed crest of the central support where the principal stress directions were known prior to testing, two single strain gauges were placed in the respective principal directions, namely the longitudinal and transverse directions. Strain gauges were used on both top and bottom surfaces of the roofing at every location chosen in order to determine both membrane and out-of-plane bending stresses.

The strain gauges had 120 ohms resistance and possessed self temperature compensation. All the single strain gauges had a gauge length of 5 mm, but the rosettes used in the vicinity of the central support fasteners had much smaller strain gauges of 2 mm gauge length so that they could be accommodated near the fastener hole.

All strain gauges were connected via a distributor box to a Huggenberger strain measuring instrument as shown in Figures 3 (b) and 5 (a). The measured strain in a direction at any location was easily converted to stress by multiplying the strain by the Young's modulus of steel. This procedure is valid until the specimen begins to yield at that location. As the measured yield stress of the roofing material was 690 MPa and the material did not show any strain hardening (see Section 2.6), the above procedure was used until a (micro) strain measurement of 3450 after which the stress at that location was assumed to be 690 MPa.

The membrane stress at any location can be obtained by averaging the corresponding surface stresses. The out-of-plane bending stress can be obtained by halving the difference in the surface stresses.

For the locations in the vicinity of the central support fasteners, the stresses in three known directions σ_a, σ_b and σ_c obtained from the rosettes were then used to determine the principal stresses σ_1 and σ_2 at that location using the equations given next (page 9).

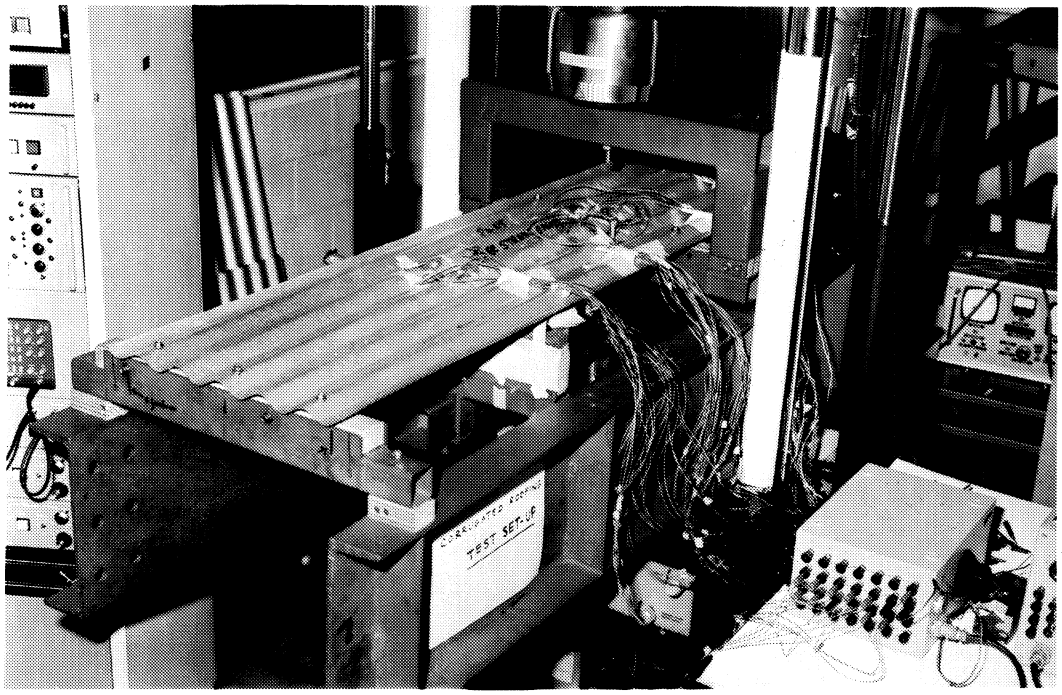

(a) Location of Strain Gauges

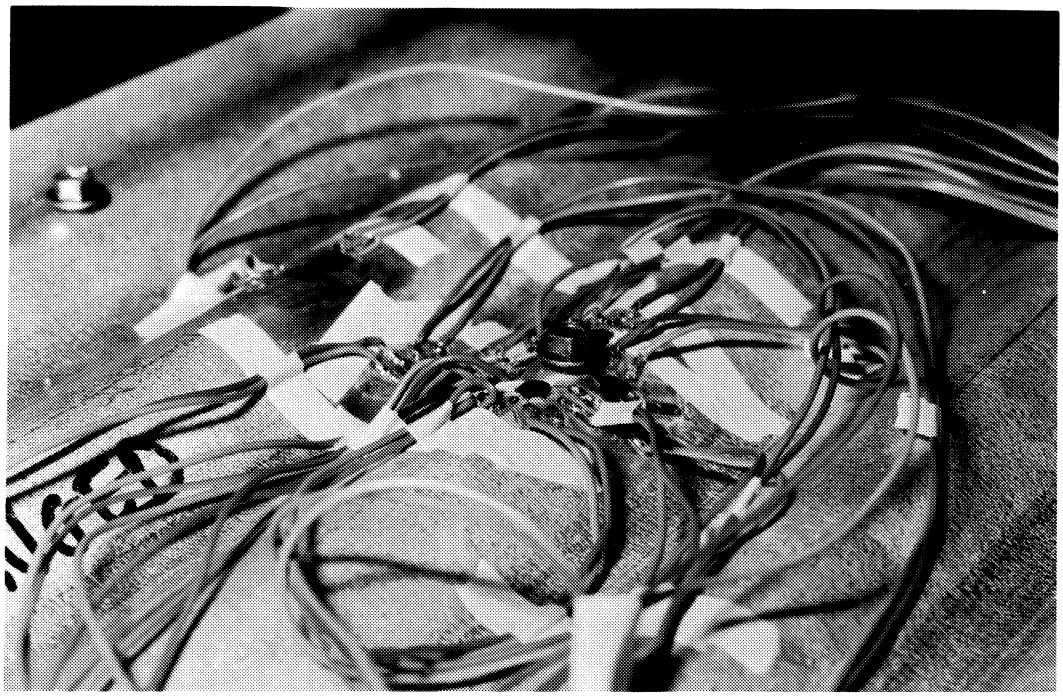

(b) Strain Gauge Rosettes in the Vicinity of Fastener hole at the Central support

Figure 5. Strain Gauged Test Specimen

$$\sigma_1 = 1/2\ [\ (\sigma_a + \sigma_c) + (\sigma_a - \sigma_c) / \cos 2\theta\ ]$$

$$\sigma_2 = 1/2\ [\ (\sigma_a + \sigma_c) - (\sigma_a - \sigma_c) / \cos 2\theta\ ]$$

$$\tan 2\theta = [\ 2\sigma_b - (\sigma_a + \sigma_c)\ ] / [\ (\sigma_c - \sigma_a)\ ]$$

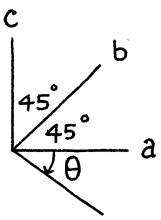

2.6 Tensile Tests to Determine the Material Properties

All the corrugated roofing used in the tests was rolled from the same coil of steel. The roofing manufacturers (LBI) supplied sample flat plates taken at intervals during the rolling of corrugated sheets. A total of 50 tensile test specimens of dimensions shown in Figure 6 were cut from the sample flat plates in both longitudinal and transverse directions of the coil. They were tested in tension under displacement control according to AS 1391 (1974) in order to determine the elastic and yield properties of the sheet material used.

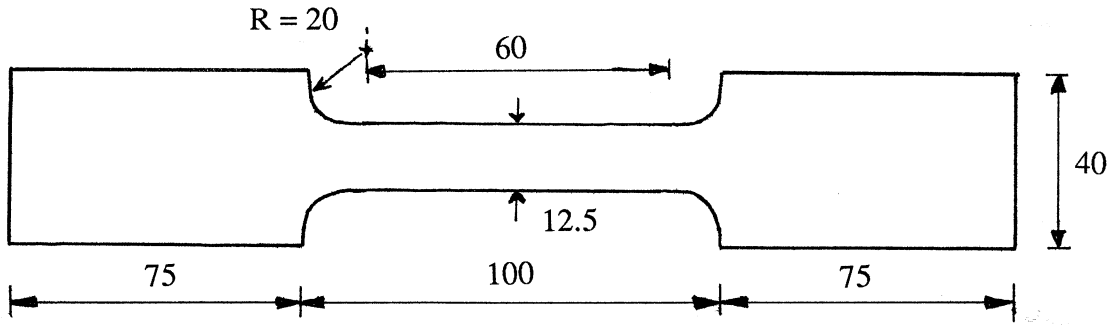

Figure 6. Dimensions of Tensile Test Specimens in mm

As recommended by the Australian standard for the Zinc or Zincalume coated steel sheets, AS 1397 (1984), the base metal thickness was used in the stress calculations. The tests on 30 specimens cut in the longitudinal direction of the coil gave a mean yield stress of 690 MPa (coefficient of variation = 2.0%) and an estimated total elongation at fracture of 0.5%. Failure occurred after a brief yielding with no strain hardening. The corresponding values from the tests on 20 specimens cut in the transverse direction of the coil were a mean of 775 MPa (coefficient of variation = 2.2%) and an elongation of 0.39%. The specimens in the latter case failed as soon as the yield load was reached. It is to be noted that as none of the specimens showed any strain hardening, the ultimate strength of the sheet material was the same as

the yield stress in either direction. Figure 7 shows some typical load-extension graphs obtained during the tensile tests.

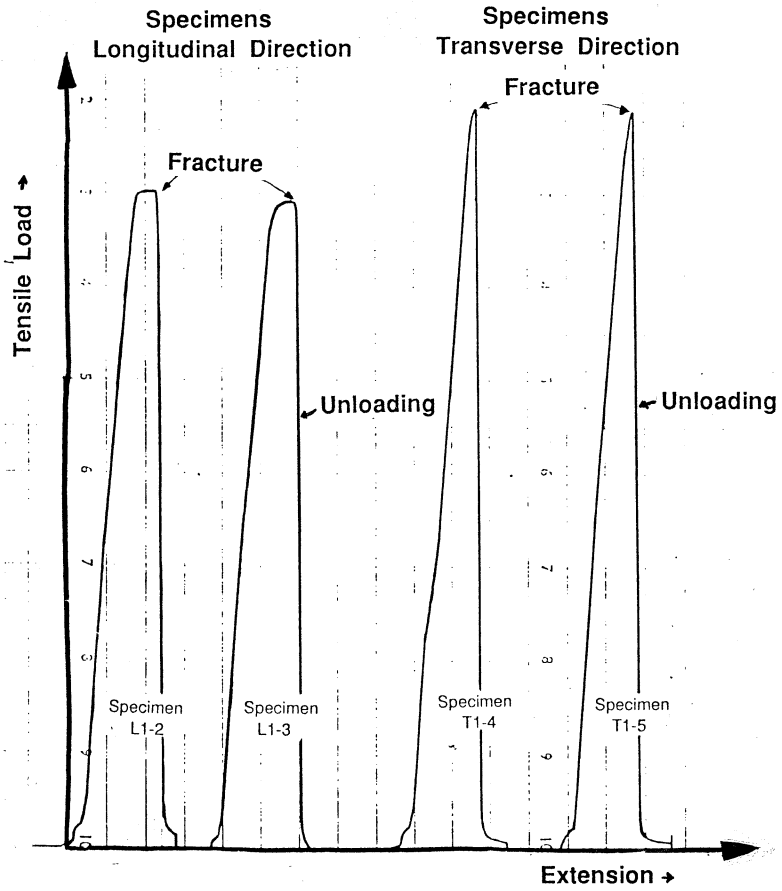

Figure 7. Typical Load-Extension Graphs from Tensile Tests

From these test results, the yield stress of the sheet material could be taken as 690 MPa, the lesser of the measured yield stresses in both directions. In fact, AS 1397 (1984) recommends testing in the longitudinal direction, presumably to account for the directional effect. The strength of the sheet material used for the tests is satisfactory as the measured minimum value of 669 MPa exceeds the guarantied strength by about 22%. However, there is some concern about the very low measured ductility, 0.5%, as AS 1397 (1984) specifies a minimum of 2% ductility. All tested specimens had a fracture surface with little or no necking, thus indicating the brittle nature of failure.

In order to study the effect of cold rolling on the material properties of the steel sheet, a limited number of test specimens of dimensions smaller than those shown in Figure 6 were cut from the crests and the sides of the corrugated roofing in the longitudinal direction and tested in simple tension. The results indicated that cold rolling did not alter the original material properties as the mean yield stress was 700 MPa and the steel was still brittle.

3. ANALYTICAL METHOD

3.1 General

An analytical study using a finite element program ABAQUS was conducted to determine the deflections and stresses in the same two-span roofing assemblies considered in the experimental analysis. ABAQUS is a multi-purpose program developed by Hibbitt et al. (1984). It is capable of static and dynamic analyses, and has a large structural element library. In this study, a doubly curved shell element was used to model the thin corrugated profile. The shell element is a four-noded quadrilateral with five degrees of freedom at each node, consisting of three displacement components and two in-surface rotation components. Although several integration points through the thickness are provided, the default value of five was chosen as it was found to be adequate for the present problem. Both nonlinear geometric and material effects were included in the analysis. Ideal elastic perfectly plastic and isotropic stress-strain behaviour was assumed. Although the program can include the effects of selfweight of the elements and any thermal effects, these effects were ignored in this analysis.

The following material properties were used in the analysis, Young's Modulus = 200,000 MPa, Poisson's ratio = 0.3 and yield stress (measured) = 690 MPa. Structural effects due to the thin Zincalume coating was considered negligible and thus the base metal thickness of 0.42 mm was used in the analysis.

3.2 Model Used in the Analysis

Because of symmetric boundary conditions and loading, roofing of one span long and one corrugation width (76 mm) was considered in the finite element analysis (FEA) of roofing fastened at alternate crests. Figure 8 illustrates the boundary and loading conditions used in this model. In the vicinity of the fastener hole, the roofing is supported by the screw head via the neoprene washer. Hence in the analysis, all the nodes within this area shown by the shaded area in Figure 8 were restrained against the Z-translation. Among the above nodes, those along the edge in contact with the screw shaft were restrained against x and y-translations as well. A model of half the corrugation width was adequate when analysing the roofing fastened at every crest. For this case, the valley was assigned the boundary conditions of the unscrewed crest shown in Figure 8 and all other conditions remained same as before.

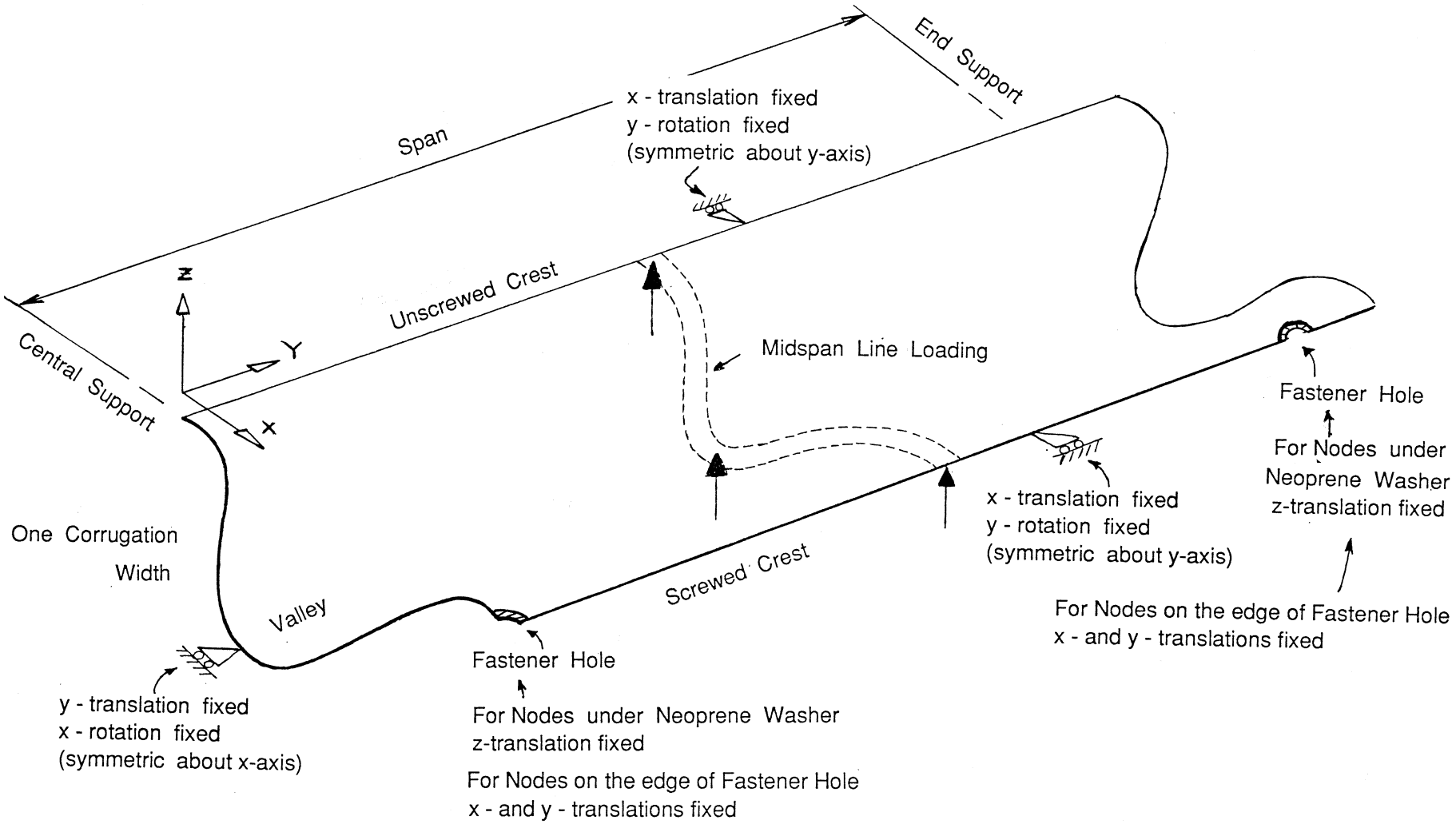

Figure 8. **Boundary and Loading Conditions for the Model used in the FEA of Corrugated Roofing Fastened at Alternate Crests**

In a finite element analysis, selection of mesh size and layout is critical. It is desirable to use as many elements as possible in the analysis. However, such an analysis will not only require excessive computer time, but also excessive time of the analyst to feed the input data and to interpret the output data. In this analysis, adequate numbers of elements were chosen both across the corrugation and along the corrugation in order to obtain sufficient accuracy of results without excessive use of computer time. Details of the mesh are given in the following paragraphs.

Each corrugation of the roofing can be idealized by arcs and tangents as shown in Figure 9. For the purposes of analysis, each arc on either side of the crest or valley, and the tangent between the crest and the adjoining valley were divided into two sections. This gave a total of 12 elements across the corrugation and such a fine mesh was used throughout the span when analysing the roofing fastened at alternate crests. There were six elements across the width in the case of roofing fastened at every crest. The position of the centre and the radius of the arc, the pitch and the depth of corrugation were the parameters used to determine the connecting point of the arc and the tangent. Based on this, all other dimensions shown in Figure 9 were calculated.

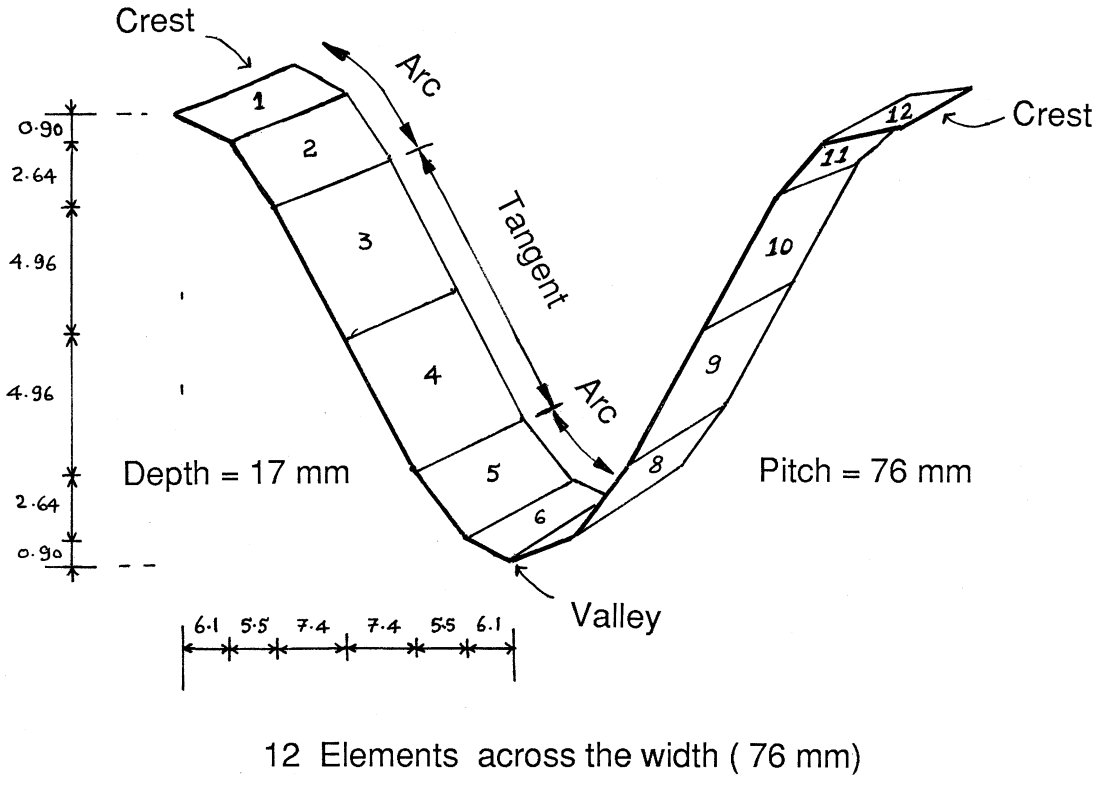

Figure 9. Idealization of Corrugated Roofing Profile for the FEA

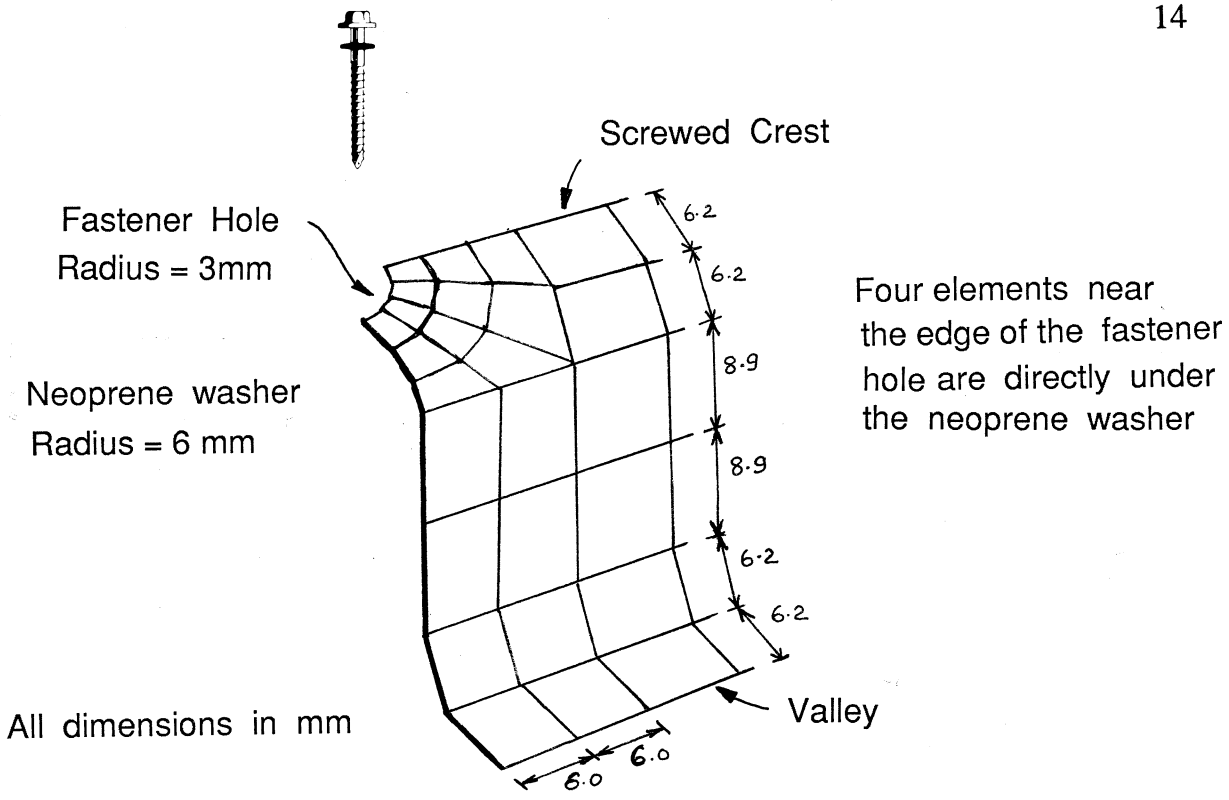

(a) Finer Mesh used in the Vicinity of the Fastener hole

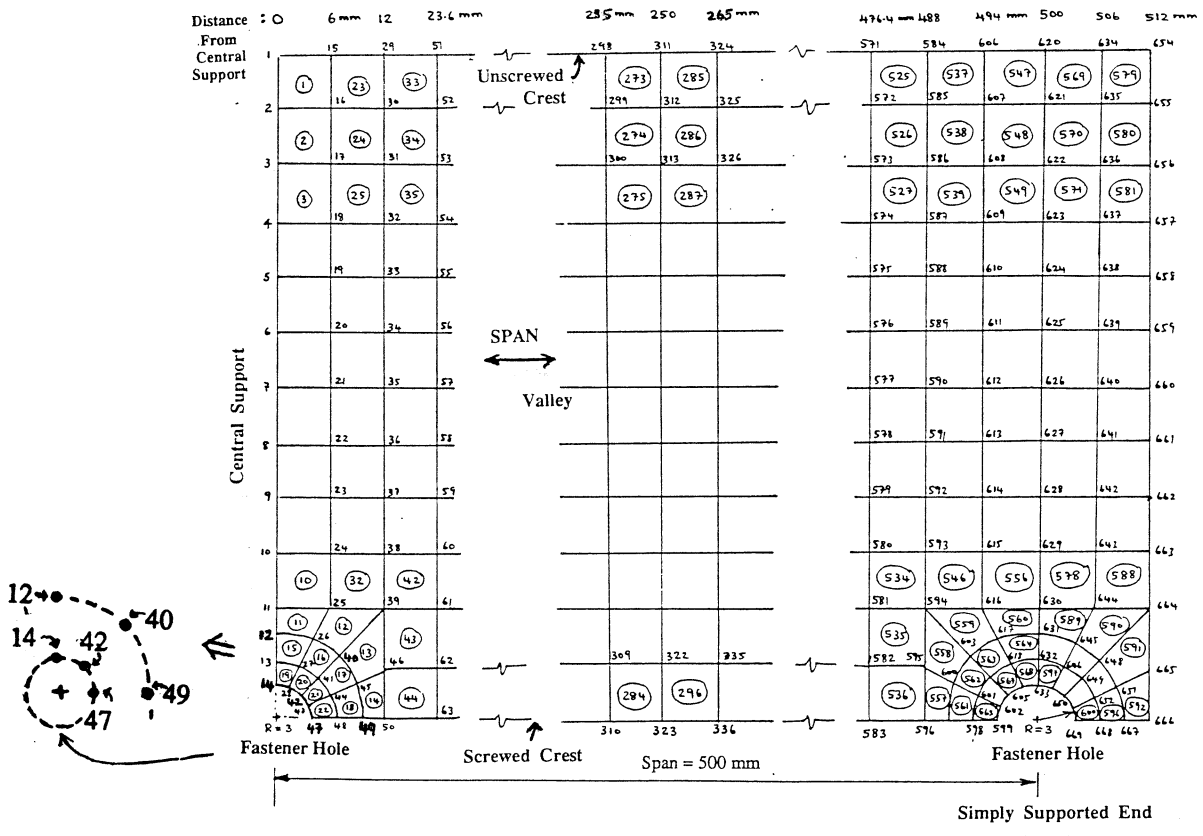

(b) Overall Mesh used in the FEA

Figure 10. Finite Element Modelling of a Two-Span Corrugated Roofing Assembly

A finer mesh as shown in Figure 10 (a) had to be used around the fastener hole due to the presence of large stresses for all the spans of roofing. As the quadrilateral shell element chosen cannot be degenerated to triangles, quadrilaterals were used even in the vicinity of the fastener hole. A separate analysis using triangular shell elements for the region around the fastener hole did not show significant differences in the results and thus quadrilateral shell elements were used throughout the span for all the cases. The selection of 12 elements across one corrugation of roofing was considered to be adequate. However, to decide on the grid-size along the span of roofing, a number of different meshes were analysed for the medium span roofing. Such mesh convergence studies indicated that the chosen mesh shown in Figure 10 (b) was satisfactory. In Figure 10 (b), an overall plan view of the mesh used in the analysis of medium span roofing is presented. As the entire span had to be modelled, the number of nodes and elements chosen were somewhat large, being 669 and 600, respectively. Same mesh was used for all the spans of roofing.

For all the spans of roofing, the aspect ratio was closer to unity for the elements closer to the supports. For the two rows of elements next to the line of midspan, the largest aspect ratio was 2.5 for all the spans. But the aspect ratio elsewhere along the span was different for each span. It was closer to unity for all the elements of short span roofing, and was closer to 2 for the arc-elements and 1.5 for the tangent-elements of medium span roofing (500 mm). The largest aspect ratio in the case of long span roofing was closer to 4 for the arc-elements.

The program permits application of loads as either point loads to the nodes or a distributed pressure to the element. In this case, midspan line loading (width = 30 mm) was simulated by applying uniform pressure loading to the rows of elements on either side of the line of midspan.

For the analytical purpose, roofing fastened at valleys under uplift wind loading can be considered to be equivalent to roofing fastened at crests (but fastened from underside to battens above) under wind loading in the opposite direction (downward). Hence the results pertaining to the case of roofing with valley fastening were obtained by using the same data file, but with loading in the opposite direction.

3.3 **Limitations of the Analysis**

Analysis was restricted to a load of 550 Newtons per fastener (N/f) for roofing fastened at alternate crests due to the local plastic buckling behaviour beyond that load.

In the analysis of roofing fastened at the crests, boundary conditions at the fastener hole were not modelled exactly. In reality, the edge of the hole is restrained only in one way in any direction. It is restrained to move against the neoprene washer and screw head, but not in the opposite direction. Similarly, in-plane movements are only restrained if the movements are against the screw shaft. However, in the analysis, they were assumed to be fully restrained both ways and thus should give conservative results.

In order to determine the stresses in the vicinity of fastener hole more accurately, an analysis of a sub-structure consisting of the small area around the fastener hole has to be conducted. However, such an analysis was not included in this investigation.

As the thin corrugated roofing is produced by cold roll-forming, initial geometric imperfections and residual stresses could be present, mainly in the transverse direction. However, they were not considered in the analysis.

3.4 **Other Details**

Although an automatic incrementation scheme is available based on the rate of convergence observed during the iterative process at each increment, the program was run using constant load increments until a preset final load was reached. It was restarted from that point to a higher load when that was required in some cases. Large number of iterations were permitted in the initial runs until a suitable set of tolerance parameters were determined. Deflections and rotations at the required nodes, and stresses on the surfaces or at the midthickness for the required elements at the centroid or at the nodes were obtained by choosing the right options.

Initially, another finite element program SAP iv developed by Bathe et al. (1974) for structural analysis was used. As SAP iv is capable of only a linear elastic small deflection analysis, it was not used later. The same mesh shown in Figure 10 was used in this analysis and the effects due to nonlinear geometry were included by an iterative process. In this process, very small load steps were chosen. The input data of the model's geometry was updated for every new step by using the deflection results from the last step. The limited results from this analysis are compared with the corresponding results from ABAQUS in Section 4.

4. RESULTS AND DISCUSSION

4.1 Roofing Fastened at Alternate Crests

4.1.1 Experimental results

When alternate crest fastening which is commonly used in cyclonic areas was used in the experiments, the roofing behaved in a manner which is seldom observed during standard bending tests. The load-deflection curves of the roofing of 650 mm span can be considered to be typical of the load-deflection curves of all the spans, and are shown in Figure 11 in which four stages of loading could be identified.

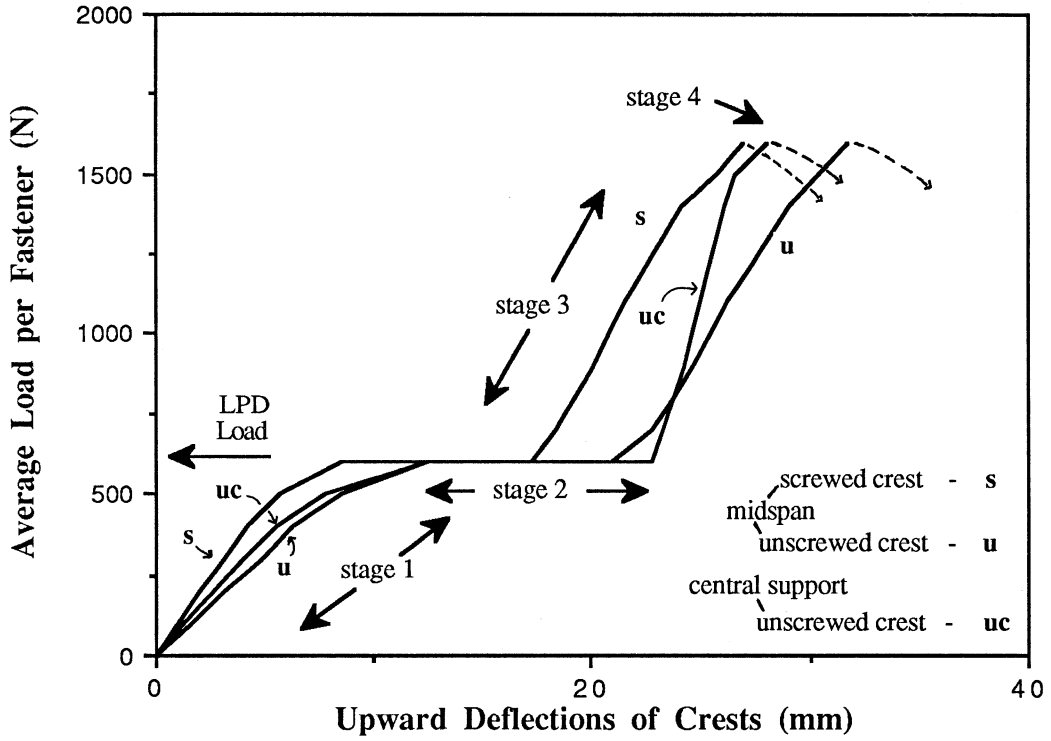

Figure 11. Load-deflection Curves for Corrugated Roofing Fastened at Alternate Crests

During the first stage, the behaviour was nonlinear elastic due to the change in geometry as the unscrewed crests deflected many times greater than the adjoining screwed crests at every cross-section. This effect was the greatest for the short span roofing. In fact, at 500 Newtons per fastener (N/f), the unscrewed crest of short span roofing deflected 10.3 mm at the midspan and 11.0 mm at the central support, compared with the adjoining screwed crest's deflections of 2.2 and 0.0 mm, respectively. This deflected mode caused severe cross-sectional distortion of roofing at the central support for all the spans (see Figure 12 (a)). However, the degree of cross-sectional distortion was less severe at the midspan as shown in Figure 12 (b).

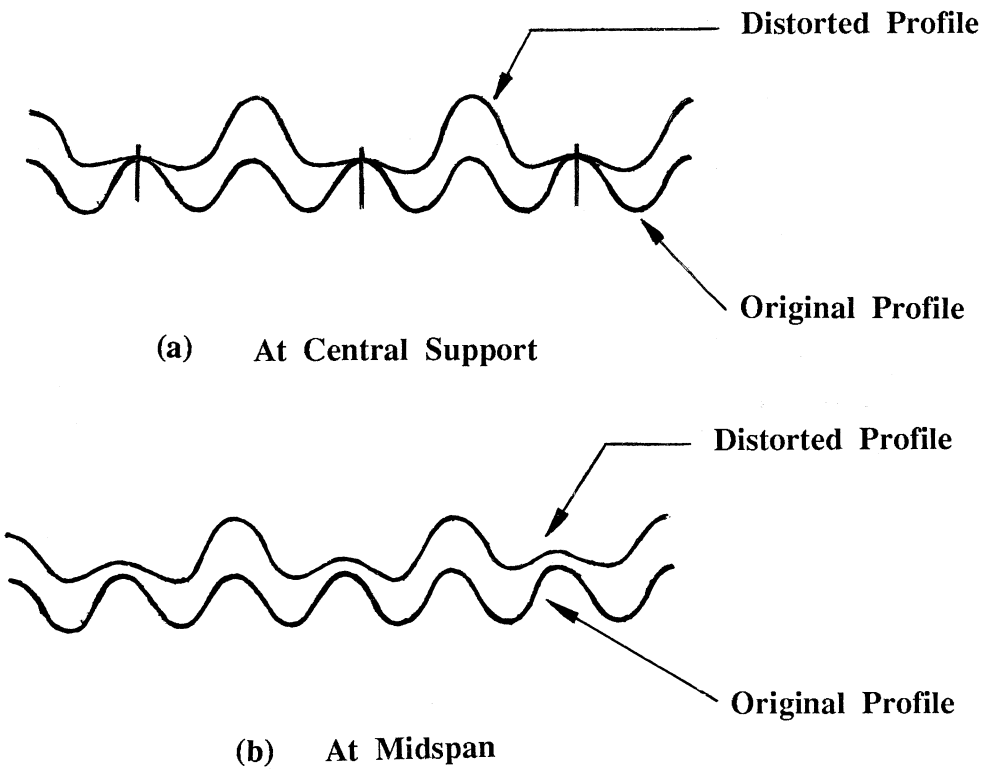

Figure 12. Cross-sectional Distortion of Corrugated Roofing Fastened at Alternate Crests

As the largest cross-sectional distortion occurred for the short span roofing, the maximum combined stress in the long span roofing at a constant load per fastener during stage 1 loading could not have been very much greater than that in the short span roofing. This could have occurred despite the presence of greater membrane stresses in the long span roofing. Confirming this, at a load between 550 and 650 N/f, a local buckle causing a flattening of the crest appeared suddenly at each of the central support fasteners for all the spans (Figure 13). Following this, large local plastic deformations (LPD) occurred causing further cross-sectional distortion to the already-deformed corrugated profile (stage 2). It is to be noted that such an initial local plastic failure occurred at approximately the same load per fastener for all the spans. Tests were repeated for each span and it was found that the results were repeatable. In fact, the variation in LPD load for each span was small and the LPD loads for the roofing of test spans 250, 500, 650 and 1000 mm could be considered to be 600, 625, 650 and 550 N/f, respectively. A similar anomalous observation in which an initial local plastic failure occurred at a smaller load for shorter spans of corrugated roofing was reported by Salaheldin et al. (1987) in their investigation on simply supported corrugated roofing under a concentrated load at midspan.

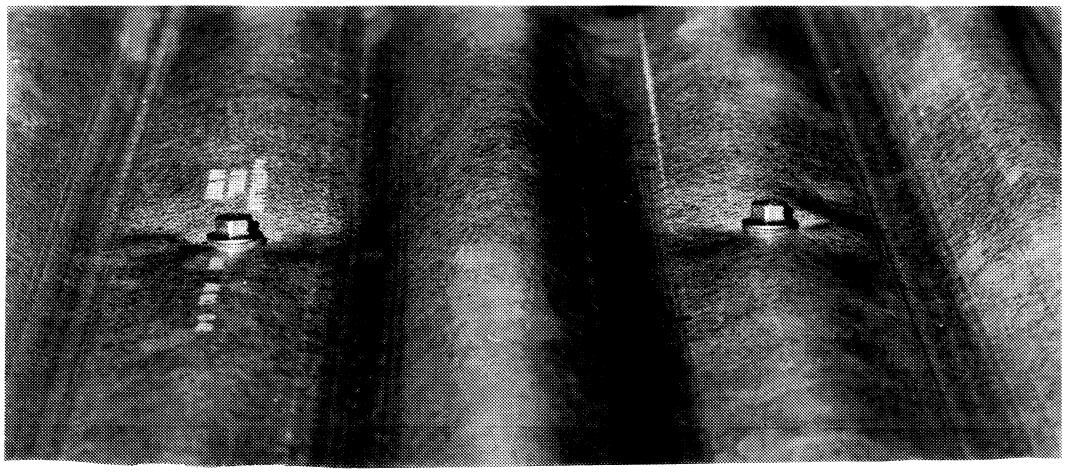

Figure 13. Local Plastic Buckling in the Vicinity of Central Support Fasteners (Stage 2 Loading)

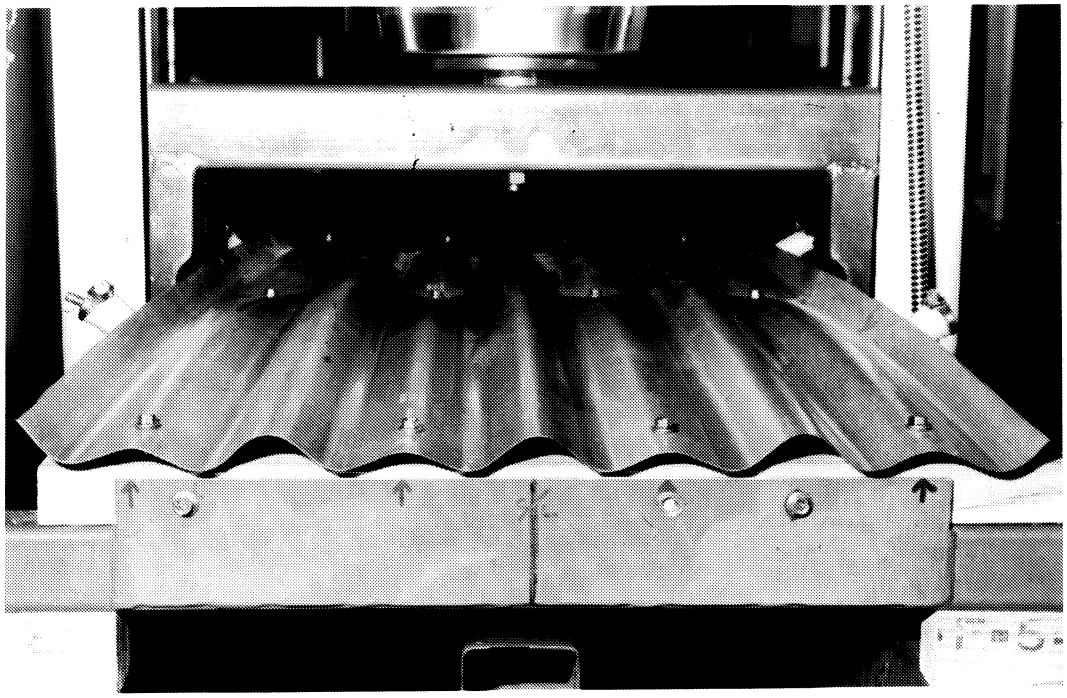

Figure 14. Corrugated Roofing During Stage 3 Loading

Although the occurrence of local plastic deformations around the central support fasteners could be considered to be an initial failure, the corrugated sheet deformed further with the load increasing steadily again during stage 3. This could be explained by the fact that once large cross-sectional distortion occurred at the LPD load, there was a redistribution of stresses across the width which was assisted by the new deeper cross-section of roofing (see Figure 14).

Finally, the crests and valleys of each midspan cross-section for most cases began to deform severely forming a global plastic mechanism across the sheet (stage 4), followed by buckling failure of the unscrewed crests at the central support, and resulting in rapid unloading. These tests could have been continued until disengagement of roofing occurred by the screw heads pulling through the roofing at the central support. However, they were discontinued once the global plastic mechanisms formed as no significant load increase was anticipated beyond the formation of mechanisms. In the case of short span roofing, global plastic mechanisms formed at both midspans, but one of the central support fasteners pulled through the roofing before the unscrewed crest could fail at the central support. These ultimate failures occurred at 1100, 1600, 2000 and 2400 N/f for roofing of long span, medium spans (650 and 500 mm) and short span, respectively. The greater ultimate strength of shorter span roofing was mainly due to the stage 3 loading. Figure 15 shows the typical global plastic mechanisms in a failed specimen.

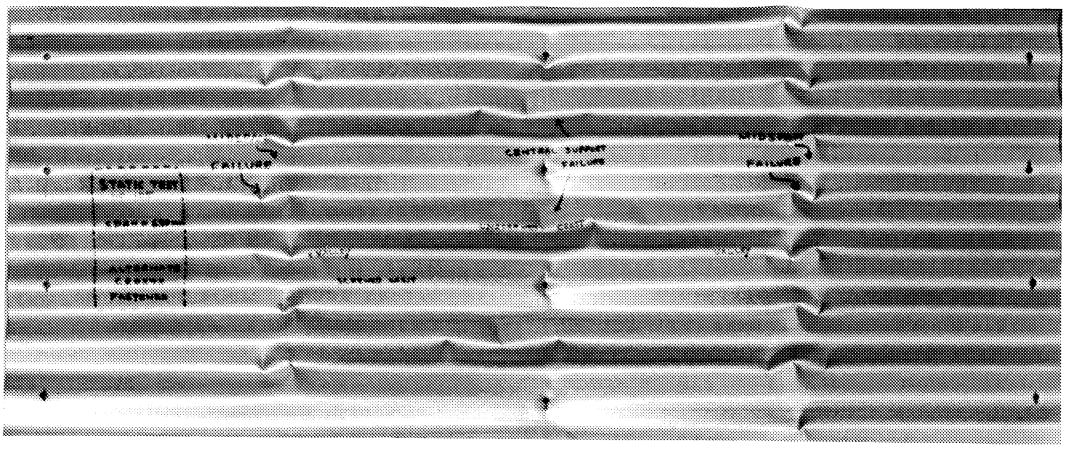

Figure 15. Ultimate Static Failure of Corrugated Roofing Fastened at Alternate Crests

Although it was found that the steel was brittle with no strain hardening during simple tensile tests on the sheet material, the behaviour of

corrugated roofing under uplift loads at midspan could be considered to be ductile which was mainly due to the redistribution of stresses associated with the change in geometry of the cross-section. Salaheldin et al. (1987) also made the same observation in their tests.

Similar observations to those mentioned in this section were also made by Beck (1978), Slogrove (1985) and Neal (1984) in their investigations on corrugated roofing of other spans. All these researchers were mainly concerned with the fatigue behaviour of roofing and thus gave very little importance to the static behaviour. Beck used an identical testing method to the one adopted in this investigation on similar corrugated roofing of 650 mm test span, but fastened with three fasteners per sheet. He observed an LPD load of 700 N/f. Both Slogrove and Neal adopted a different testing method described by Reardon (1980). Slogrove carried out six static tests on nominally identical corrugated roofing used in the present series of tests. The roofing was fastened at alternate crests with four screws across the width in his laboratory model that represented an actual internal span of 1040 mm. The LPD load in his tests was between 500 and 600 N/f and the ultimate failure load between 1500 and 1800 N/f. Neal's tests were on New Zealand Fletcher Brownbuilt's galvanized corrugated roofing (G550, 0.40 mm bmt, 19 mm corrugation depth and 76 mm pitch) that was fastened with nails at alternate crests. Only two fasteners were used in Neal's laboratory model which was constructed to model an actual span of 1200 mm. The mean of the LPD load from his 12 static tests was 570 N/f and the ultimate failure load based on the withdrawal strength of the nails was approximately 1800 N/f. All these test results obtained by other researchers show that the LPD load was between 500 and 700 N/f for corrugated roofing profiles of different spans fastened with screws or nails.

4.1.2 **Comparison of analytical and experimental results**

The FEA was conducted for the roofing of short span, long span and only one of the medium spans (500 mm), and thus comparison of analytical and experimental results are made only for these three spans of roofing. As analysis was not continued beyond the local plastic buckling failure at the central support fasteners, analytical results are available only up to a loading of 550 N/f. Figure 16 presents the deflection results from both the FEA and experiments at 500 N/f in a format that illustrates the cross-sectional distortion across the width of the roofing at midspan and central support. The overall agreement between the two results is reasonably good and thus validates the use of FEA to study the behaviour of corrugated roofing. The FEA confirms all the experimental observations made earlier regarding the cross-sectional distortion during stage 1.

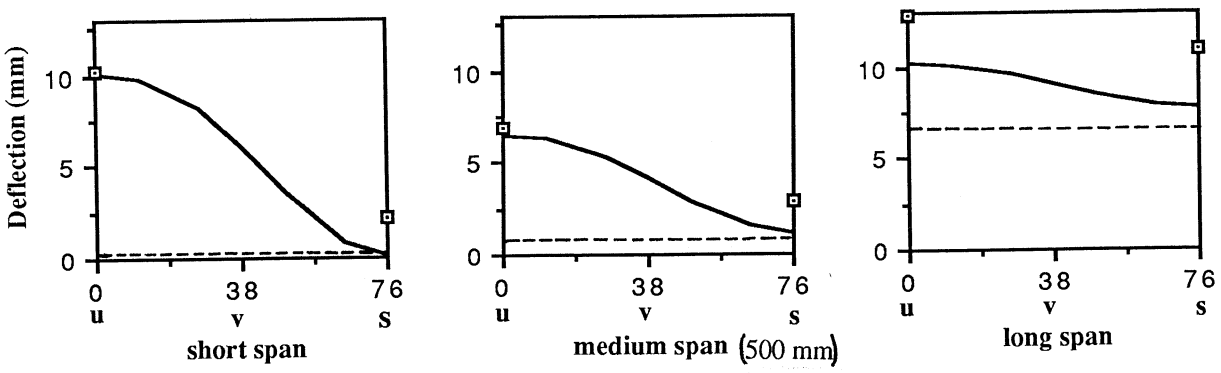

(a) Upward Deflection at Midspan at 500 N/f : FEA, Experiments and SET

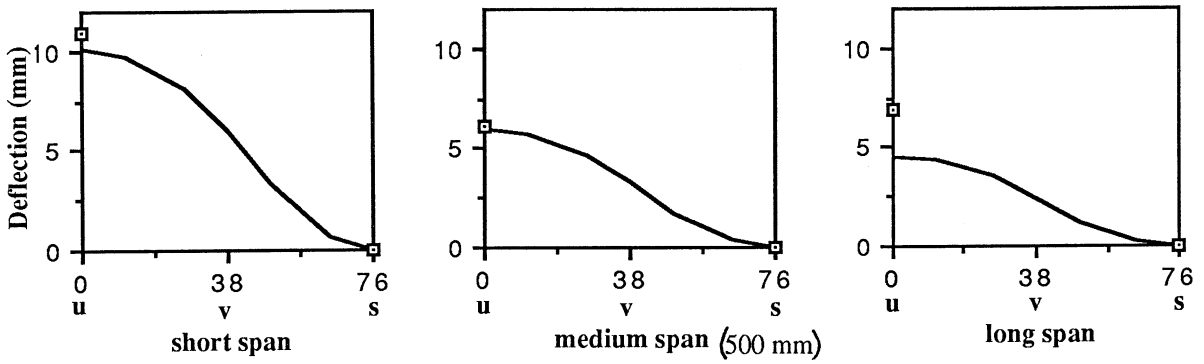

Note : SET assumes no deflection at central support

(b) Upward Deflection at Central Support at 500 N/f : FEA and Experiments

Note. s - Screwed Crest
u - Unscrewed Crest
v - Valley

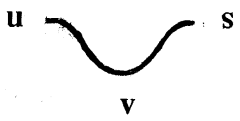

FEA ——
Experiments ▫
SET ------

Figure 16. Upward Deflections across one corrugation width for Corrugated Roofing Fastened at Alternate Crests

The results obtained using the simple engineering theory (SET) are also included in Figure 16. The SET results were calculated using the following formula that is based on simple pure bending assumptions and a constant second moment of area of roofing.

Midspan Deflection = $W L^3 / 110. E I$

where W = Midspan line load = Central support reaction/1.375
L = Span of the roofing
E = Young's Modulus, 200,000 MPa for steel
I = Second Moment of area of corrugated roofing

The value of 'I' can be calculated from the following formula in Perry's Engineering Manual (Perry and Perry, 1959).

$$I = 64\,(b_1 h_1^3 - b_2 h_2^3) / 105$$

where $b_1 = (B + 2.6\,t)/4$

$b_2 = (B - 2.6\,t)/4$,

B = Pitch of Corrugations = 76 mm

$h_1 = (H + t)/2$

$h_2 = (H - t)/2$,

H = Depth of Corrugation = 17 mm

and t = Thickness of Corrugated Roofing = 0.42 mm

This formula gave a value of 16.6 x 10^3 mm^4 / metre width for 'I' which agrees very closely with the value of 16.3 x 10^3 calculated using integration from basic principles for the exact cross-section of roofing, consisting of arcs and tangents. When the arcs were divided into two sections as shown in Figure 9 and considered as flat sections, the corresponding value calculated using integration was 15.9 x 10^3. As the experiments clearly revealed the significant changes in the cross-section of roofing, the assumption of constant second moment area of roofing until failure or even up to a lesser load of 500 N/f will obviously be incorrect, as will other basic pure bending assumptions. Hence, in contrast to the FEA, the SET results do not agree with experimental results. In particular, the SET is unable to predict the greater deflections of unscrewed corrugations as seen in Figure 16.

The results shown in Figure 16 indicate that the maximum midspan upward deflection of roofing occurs at the unscrewed crest and is of the same order for short and long span roofing at the same load per fastener. However, the recommended allowable deflection for roofing subjected to wind forces is span/90 according to AS 1562 (SAA, 1980). This means that the allowable deflection for long span roofing is four times that of short span roofing. Hence an anomalous situation may arise in this case when alternate crests are fastened.

Figures 17 (a) to (c) present the deflection results in a different format to that of Figure 16. In these figures, the experimental results up to the ultimate failure load and the analytical results up to the LPD load are presented for roofing of test spans 250, 500 and 1000 mm in that order. The experimental load-deflection graphs of other medium span roofing (650 mm) has been already presented in Section 4.1 and analytical results are not available for that case.

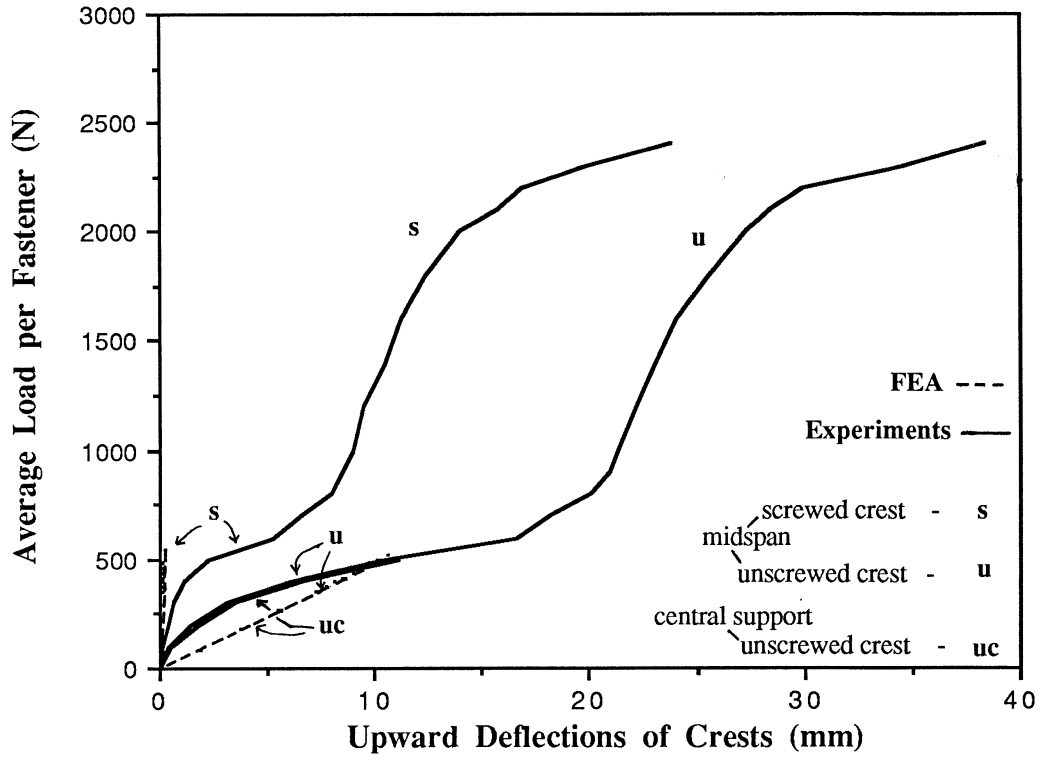

(a) Short Span Roofing (test span = 250 mm)

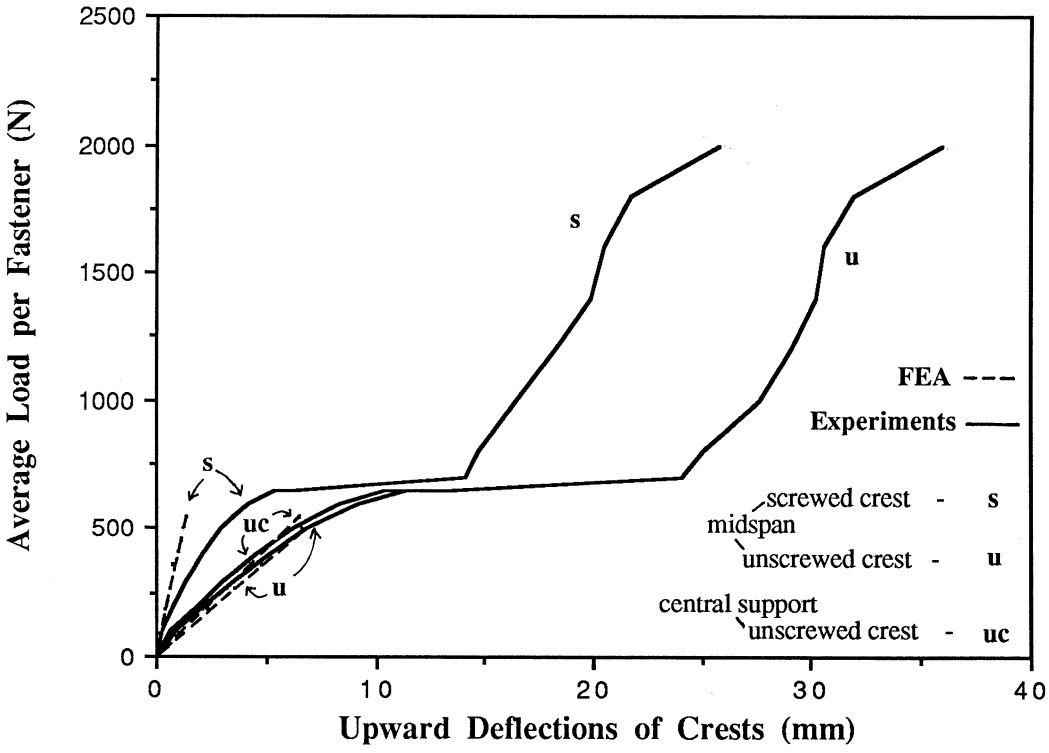

(b) Medium Span Roofing (test span = 500 mm)

Figure 17. Load-deflection Curves for Corrugated Roofing Fastened at Alternate Crests

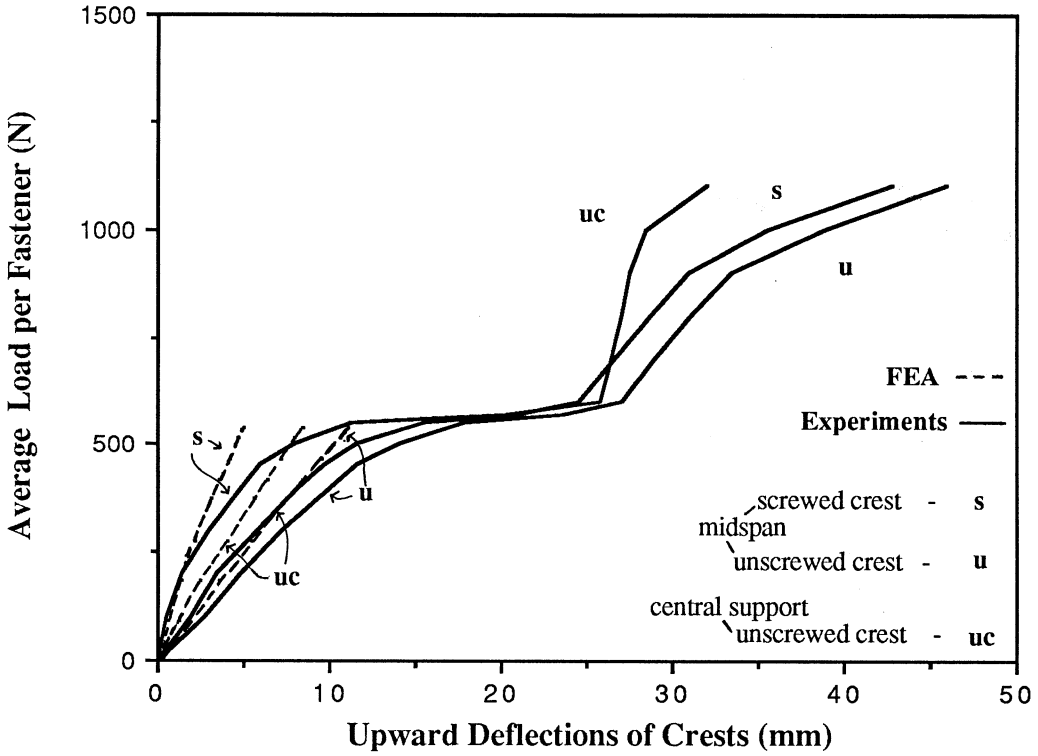

(c) **Long Span Roofing (test span = 1000 mm)**

Figure 17. Load-deflection Curves for Corrugated Roofing Fastened at Alternate Crests

The limited analytical results obtained earlier in this investigation from the other finite element program SAP iv are not used in the comparison of results. However, it is to be noted that they are in good agreement with the results from ABAQUS for all the spans. In the case of medium span roofing (500 mm) at 500 N/f, the upward deflections from SAP iv analysis after accounting for the nonlinear geometric effects (see Section 3.4) are 1.1, 6.7 and 6.4 mm for screwed and unscrewed crests at midspan, and unscrewed crest at central support, respectively. These deflection results compare very well with the corresponding results of 1.2, 6.6 and 6.0 mm from ABAQUS.

Tables 1 and 2 present the stresses in the top and bottom surfaces of the roofing at midspan and central support at a load of 500 N/f as obtained from the FEA and compare with the available results from tests on strain gauged specimens. There is reasonable agreement between the two results. The stresses at other loads up to 550 N/f are given in Tables A1 to A6 of Appendix A for all three spans. From these tables of surface stresses, the membrane stress at any location can be obtained by averaging the corresponding top and bottom surface stresses, and the out-of-plane bending stress by halving the difference in the surface stresses, as already stated in Section 2.5.

Table 1 (a). Midspan Longitudinal Bending Stresses at 500 N/f for Roofing Fastened at Alternate Crests (MPa)

Test Span (mm)		Crests, Valleys SET	Unscrewed Crest FEA	Unscrewed Crest Expt.	Valley FEA	Valley Expt.	Screwed Crest FEA	Screwed Crest Expt.
250	T	49	116	67	-36	-76	-71	105
	B	49	-34	53	-100	-88	205	96
500	T	97	125	-	-104	-	42	-
	B	97	27	-	-123	-	172	-
1000	T	194	199	182	-195	-194	180	234
	B	194	150	160	-206	-213	223	222

Table 1 (b). Midspan Transverse Bending Stresses at 500 N/f for Roofing Fastened at Alternate Crests (MPa)

Test Span (mm)		Crests, Valleys SET	Unscrewed Crest FEA	Unscrewed Crest Expt.	Valley FEA	Valley Expt.	Screwed Crest FEA	Screwed Crest Expt.
250	T	-	249	206	99	83	-465	-435
	B	-	-242	-230	-105	-51	475	418
500	T	-	159	-	19	-	-225	-
	B	-	-152	-	-26	-	232	-
1000	T	-	70	-25	-6	66	-89	-181
	B	-	-61	-54	-4	57	97	67

Table 2. Central Support Bending Stresses at 500 N/f for Roofing Fastened at Alternate Crests (MPa)

		LONGITUDINAL STRESSES					TRANSVERSE STRESSES				
Test Span (mm)		Crests, Valleys SET	Unscrewed Crest FEA	Unscrewed Crest Expt.	Valley FEA	Valley Expt.	Crests, Valleys SET	Unscrewed Crest FEA	Unscrewed Crest Expt.	Valley FEA	Valley Expt.
250	T	58	52	6	84	55	-	251	210	115	70
	B	58	-97	2	22	30	-	-251	-224	-110	-40
500	T	117	-29	-	114	-	-	170	-	40	-
	B	117	-128	-	99	-	-	-171	-	-36	-
1000	T	234	-158	-156	228	227	-	122	220	29	98
	B	234	-225	-149	225	264	-	-126	-162	-24	96

Note. 1. FEA - Finite Element Analysis
2. SET - Simple Engineering Theory
3. Expt. - Experimental Results
4. T, B - Top, Bottom Surfaces of Roofing

The following discussions are made in general terms based on the stress results listed in Tables 1 and 2. The results indicate the presence of local out-of-plane bending stresses in both longitudinal and transverse directions in addition to the longitudinal membrane stress due to the deflected mode of roofing mentioned earlier. The FEA shows that despite larger membrane stresses in the long span roofing, maximum combined longitudinal stress on the surface of long span roofing at midspan (223 MPa at 500 N/f) is not very much greater than the corresponding stress in the short span roofing (205 MPa at 500 N/f) due to the presence of a greater out-of-plane bending component in the case of shorter spans. The corresponding experimental values of 222 and 96 MPa, respectively, do not verify the above point exactly, but the stress in the short span roofing is certainly not 25% of the stress in long span roofing as calculated by SET.

As anticipated from the deflected modes shown in Figure 12, there are significant transverse bending stresses all along the span. These stresses are the greatest along the screwed crest for all the spans. The surface transverse bending stresses at any location are almost equal in magnitude, but are opposite in sign. The top surface stress at the unscrewed crest along the span is tensile whereas that at the screwed crest is compressive. This could be explained easily using the distorted shapes shown in Figure 12. As the FEA indicates, large transverse bending stresses (475 MPa at 500 N/f) are present even at the midspan in the short span roofing, especially at the screwed crest, and are considerably greater than the corresponding stresses in the long span roofing (97 MPa at 500 N/f) as seen in Tables 1 (b) and 2. Such large transverse bending stresses prevail in the shorter span roofing due to the greater cross-sectional distortion.

The transverse bending stresses at the unscrewed crest are smaller than the corresponding stresses at the screwed crest, but both stresses increase nearer the central support. In fact, the latter stresses are at yield values at the central support for all three spans at 500 N/f as shown in Table 3. This can be explained by the greater cross-sectional distortion at the central support, as shown in Figure 12. Experimental results confirm all these observations regarding transverse bending stresses very well. The above observations regarding stresses in the roofing are not predicted by simple engineering theory which makes it unsuitable for use in determining the maximum bending stresses, particularly for shorter spans of roofing (see Tables 1 and 2)

Table 3. Stresses in the Vicinity of Central Support Fasteners at 500 N/f for Roofing Fastened at Alternate Crests (MPa)

Test Span (mm)		Node 14 Longl. FEA	Node 14 Transv. FEA	Node 14 Transv. FEA	Node 12 Longl. FEA	Node 12 Longl. Expt.	Node 12 Transv. FEA	Node 12 Transv. Expt.	Node 12 Transv. FEA	Node 42 Longl. FEA	Node 42 Transv. FEA	Node 42 Transv. FEA
250	T	-425	-783		-276	155	-553	9		-304	-247	
	B	313	782		83	-58	307	-100		-6	153	
	PT	-412	-797	(690)	-264	155	-566	9	(490)	-372	-179	(322)
	PB	305	790	(690)	32	-57	358	-101	(343)	-9	155	(160)
500	T	-410	774		-252	-	-370	-		-318	-195	
	B	157	744		-34	-	152	-		-107	94	
	PT	-388	-797	(690)	-247	-	-376	-	(331)	-366	-148	(319)
	PB	148	752	(690)	-59	-	178	-	(214)	-107	94	(174)
1000	T	-455	-733		-294	227	-260	361		-401	-154	
	B	-3	660		-136	-354	93	-520		-227	56	
	PT	-415	-773	(669)	-302	226	-253	362	(280)	-431	-125	(384)
	PB	-8	665	(671)	-146	-353	104	-521	(217)	-228	57	(261)

Test Span (mm)		Node 40 Longl. FEA	Node 40 Transv. FEA	Node 40 Transv. FEA	Node 47 Longl. FEA	Node 47 Transv. FEA	Node 47 Transv. FEA	Node 49 Longl. FEA	Node 49 Longl. Expt.	Node 49 Transv. FEA	Node 49 Transv. Expt.	Node 49 Transv. FEA
250	T	-299	-558		73	52		-230	75	-294	-690	
	B	96	599		-306	-113		11	-83	408	690	
	PT	-296	-560	(485)	80	45	(69)	-165	76	-359	-690	(311)
	PB	92	602	(562)	-345	-74	(315)	-34	-87	453	690	(471)
500	T	-285	-404		-139	-3		-262	-	-169	-	
	B	-54	388		-312	-78		-117	-	221	-	
	PT	-278	-411	(363)	-139	-3	(137)	-286	-	-145	-	(248)
	PB	-55	389	(419)	-325	-65	(298)	-130	-	234	-	(320)
1000	T	-342	-304		-361	-49		-373	-210	-137	-651	
	B	-168	254		-415	-77		-257	-318	153	690	
	PT	-358	-288	(329)	-362	-48	(340)	-382	-205	-128	-656	(336)
	PB	-169	254	(368)	-421	-71	(391)	-260	-322	156	690	(363)

Note. 1. FEA - Finite Element Analysis
2. Expt. - Experimental Results
3. T, B - Stresses on Top, Bottom Surfaces of Roofing
4. PT, PB - Principal Stresses on Top, Bottom Surfaces of Roofing
5. von Mises equivalent stress from FEA is given inside brackets.

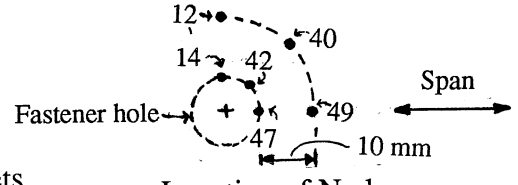

Location of Nodes

The analytical longitudinal and transverse bending stresses in the vicinity of the central support fastener hole (at nodes 12, 14, 40, 42, 47 and 49) and the available experimental stresses for short, medium (500 mm) and long span roofing at a load of 500 N/f are presented in Table 3. The stresses at other loads up to 550 N/f are given in Tables B1 to B3 of Appendix B. These tables also present the corresponding principal stresses from the FEA and experiments, the former being taken directly from the FEA output and the latter by calculations using the equations given in Section 2.5. The FEA uses the von Mises criterion for yielding and thus the von Mises equivalent stress at each load level is also included in the tables.

As the material yield stress is 690 MPa, the FEA reveals that by 500 N/f, yielding has begun at some locations around the central support fasteners for all three spans. The results from tests on short and long span strain gauged specimens confirm the yielding around the central support fasteners at the same load level. However, the points of yielding are not the ones indicated by the FEA. This discrepancy could have been due to the fact that exact boundary conditions at the edge of the fastener hole were not simulated in the FEA (see Section 3.3). As only two tests were conducted on strain gauged specimens, it is quite possible that the discrepancy could have been mainly due to experimental errors. These errors could have arose in the installation of strain gauges on the top and bottom surfaces directly on top of each other within the limited space available around the pre-drilled fastener hole, and also in mounting the strain gauged specimen. They could also have been caused by malfunctioning of some of the strain gauge channels used. However, the tables present all the results as obtained. During the test on long span strain gauged specimen, the bond between the gauges and the roofing did not permit measurement at the central support beyond 500 N/f, that is, once large localized deformations took place at this location.

The FEA indicates that the shear stress component at any point in the vicinity of central support fastener hole is rather small compared with the respective longitudinal and transverse stresses, and thus the principal stress directions almost coincide with the longitudinal and transverse directions (the maximum difference being 20 degrees in very rare cases). This is reflected by the fact that the principal stresses at any point and the respective longitudinal and transverse components being almost equal as shown in Table 3. Although the strain gauge results do not agree very well with the FEA results, they confirm very well the above observation. It is to be noted that the strain gauge results regarding principal stresses and directions at the locations around the central support fasteners were obtained independently using three-arm rosettes consisting of gauges at 45 degrees.

Both experimental and FEA results indicate that as the loading is increased beyond 500 N/f, yielding spreads to other points in the small region around the fastener hole. Once the local yielding developed sufficiently, it could be assumed that local buckles are likely to develop under the fastener heads, followed by large local plastic deformations. This is in agreement with the experimental observation of a sudden local buckle and subsequent local plastic deformations which occurred in the range of 550 to 650 N/f for all the spans.

The strain gauge measurements show that the region around the fastener continued to yield during the local plastic deformations following the buckle (stage 2). Beyond the stage 2 loading, analytical results are not available to explain the experimental observation of stage 3 loading. However, the strain gauge measurements clearly indicate that redistribution of stresses occurred during stage 3 loading, despite continued yielding of a small area around the central support fasteners. The stress pattern around the fastener hole is rather complicated, but in general, the stresses are of bending type with compression on the top surface and tension on the bottom surface due to significant local out-of-plane bending and global bending actions. It is to be noted that during the simple tensile tests where the load action was purely membrane, the steel used for the roofing fractured with very little yielding. However, the roofing exhibited sufficient ductility and did not fracture at the central support fasteners despite reaching yield values. This was probably because, in addition to the redistribution of stresses in that area, the steel could have had sufficient ductility under such bending type stresses.

Stresses in the midspan and the unscrewed crest of the central support steadily increased during stage 3 until the midspan stresses reached yield values at a load closer to the respective ultimate load value for each span. The membrane longitudinal stresses at both screwed and unscrewed crests of the midspan approached +690 MPa (tensile) whereas at the midspan valley the stresses approached -690 MPa (compressive). For example, at 1000 N/f the measured stress values at the top and bottom surfaces for long span roofing were 690 and 661 MPa at the midspan screwed crest, 505 and 459 MPa at the midspan unscrewed crest, -632 and -675 MPa at the midspan valley and -537 and -517 MPa at the central support unscrewed crest. This resulted in buckling of valleys at midspan and forming the global plastic mechanism across the width at midspan. Soon after this, the corresponding stress at the unscrewed crest of the central support also reached -690 MPa (compressive) and the unscrewed crests failed by buckling.

4.2 Roofing Fastened at Alternate Crests with Cyclone Washers

4.2.1 Experimental results

For all the spans, the use of 1 mm thick cyclone washers shown earlier in Figure 2 restricted the initial cross-sectional distortion that would have formed if washers were not used. However, as the loading was increased, the thin steel washers were unable to maintain that restriction. The local plastic deformations still occurred, but at higher loads of 1300, 1000, 900 and 750 N/f, for roofing of short span, medium spans of 500 and 650 mm, and long span, respectively. It is to be noted that the LPD load is now significantly greater for shorter spans and thus the anomalous observation regarding the LPD load being the same for all the spans of roofing is non-existent. The typical experimental load-deflection curve is still similar to that shown in Figure 11, but with a greater LPD load.

Beyond the LPD load, the load increased steadily again in a similar way to that in the case of roofing without washers. At this stage the washers at the central support had deformed so severely that they were totally ineffective. The ultimate failure occurred in a similar manner to that of roofing without cyclone washers at approximately the same failure load, for example, at 1100 N/f in the case of long span roofing. The global plastic mechanisms which formed in this case were similar to those shown in Figure 15 for the case of roofing without washers. In summary, the effect of the use of cyclone washers could be considered to be longer stage 1 loading and correspondingly shorter stage 3 loading for each span. Figure 18 presents the load-deflection curves for all the spans in this case.

4.2.2 Comparison of analytical and experimental results

Analysis of roofing with cyclone washers can be conducted by including the additional support provided by the bigger cone shaped neoprene washer, and also by the edges of steel washer to the sides of the corrugation. It is to be noted that as the washers are relatively thin, they cannot totally prevent the upward deflection of the corrugations. In fact, the longitudinal edges of the washer deflected upwards to some extent along with the corrugation even during the initial stages of loading. A realistic boundary condition at the support along the longitudinal edges of the washer falls between a fixed support condition and a no support condition. However, an approximate analysis assuming fixed boundary conditions was conducted for the medium span roofing (500 mm).

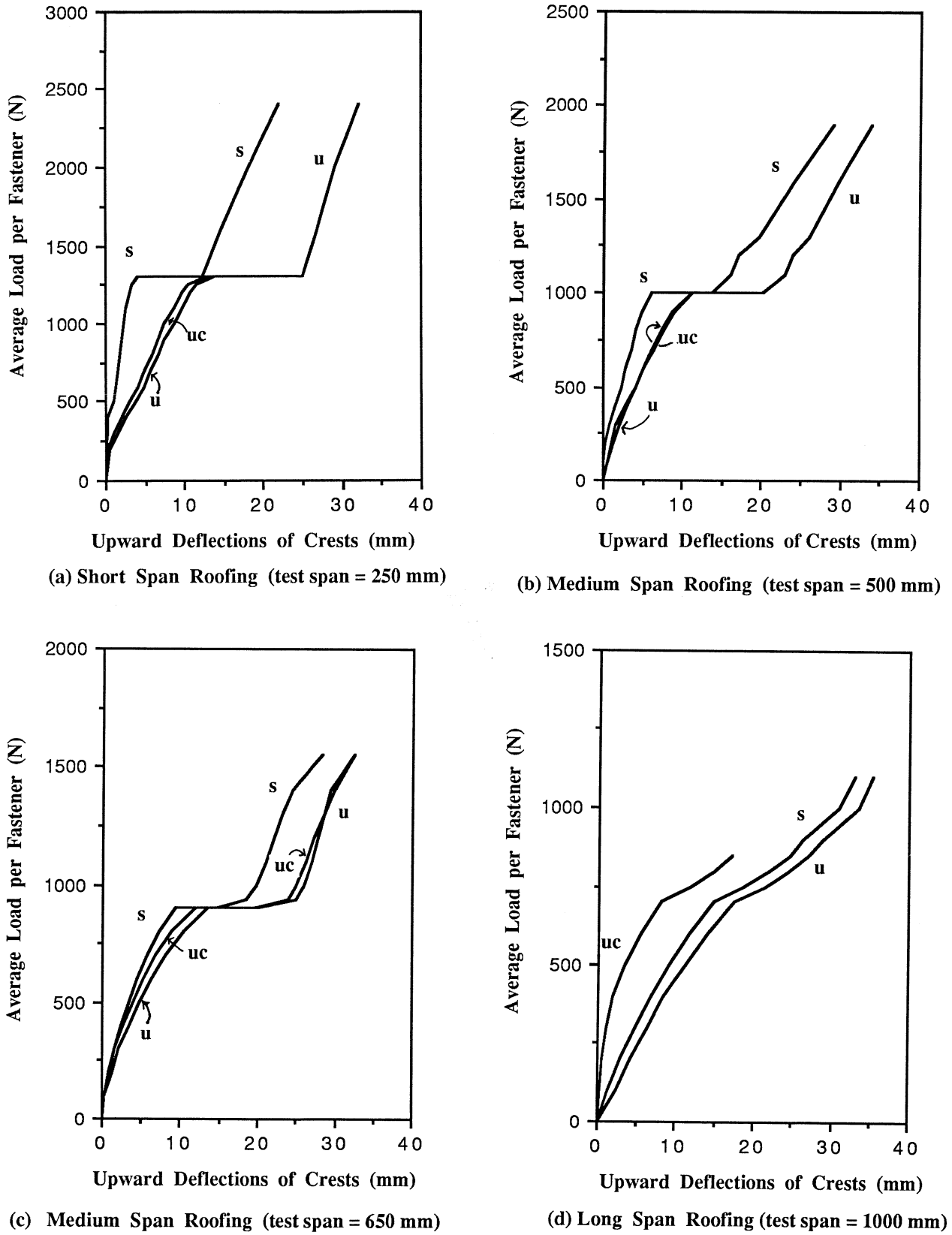

Note. **s** - midspan screwed crest **u** - midspan unscrewed crest
uc - central support unscrewed crest

Figure 18. Load-deflection Curves for Corrugated Roofing Fastened at Alternate Crests with Cyclone washers

This analysis was conducted using the finite element program SAP iv. The deflection results from this analysis at a load level of 500 N/f are compared with the corresponding experimental results in Table 4. For the purposes of comparison, both the analytical results using the same finite element program and the experimental results at the same load level obtained for the same roofing, but fastened without washers are also included in Table 4. The results reveal that the upward deflection of the unscrewed crest is reduced when washers are used and thus the cross-sectional distortion is also reduced.

Table 4. Effect of Cyclone Washers on Upward Deflections Medium Span Roofing (500 mm) - At 500 N/f

	Upward Deflection (mm)			
	With Cyclone Washers		Without Cyclone Washers	
	Experiments	Analysis	Experiments	Analysis
u	4.8	5.2	6.9	6.7
s	2.5	0.9	3.0	1.1
uc	4.5	5.0	6.2	6.4

Note. 1. **u** = Unscrewed Crest at midspan
2. **s** = Screwed Crest at midspan
3. **uc** = Unscrewed Crest at Central Support

The stress results from the same analysis at a load level of 500 N/f for the roofing fastened with and without washers are compared in Table 5. The overall stress levels in the roofing are reduced when washers are used. In particular, the stresses in the vicinity of central support fasteners shown by italic numbers in the table are reduced significantly and are now well below the yield values at 500 N/f. This explains why the LPD load was increased for all the spans of roofing during tests. The greatest increase in LPD load was for the short span roofing (from 600 to 1300 N/f) as the largest cross-sectional distortion that occurred in this case without washers was reduced very much when washers were used.

The crest region within the washer appears to be well protected from high localized stresses, but significantly higher stresses are instead present at locations away from the screw hole where the edge of the steel washer is resting on the roofing. As seen from Table 5, the transverse bending stresses at the central support valley are increased when washers are used. This is indicative of the higher stresses that are

present in the roofing under the edge of the washer which is located near the central support valley. In fact, the maximum longitudinal and transverse bending stresses at the edge of the washer are 275 and 510 MPa, respectively, at the same load level. This observation regarding the stress levels in the vicinity of the central support fasteners could mean that premature fatigue cracks will not develop under the screw head until the increased LPD load is reached when cyclone washers are used. However, cracking or tearing may develop under the edge of the washer away from the screw holes.

Table 5. Effect of Cyclone Washers on Stress Medium Span Roofing (500 mm) - At 500 N/f

	Midspan Stresses (MPa) Longitudinal		Midspan Stresses (MPa) Transverse		Central Support Stresses (MPa) Longitudinal		Central Support Stresses (MPa) Transverse	
	Washers with	Washers without	Washers with	Washers without	Washers with	Washers without	Washers with	Washers without
usc T	120	124	105	153	17	28	137	220
B	54	30	-94	-142	-64	-107	-136	-221
val T	-108	-109	-66	-60	93	91	151	41
B	-78	-83	53	47	-6	71	-149	-39
sc T	6	-4	-238	-281	*-90*	*-349*	*-29*	*-617*
B	146	162	252	295	*-60*	*104*	*37*	*385*

Note. 1. usc = Unscrewed Crest 2. val = Valley
3. sc = Screwed Crest 4. T, B = Top, Bottom Surfaces of Roofing

It is to be noted that the above observations in this section are based on a simple linear elastic analysis using approximate boundary conditions. However, these analytical results appear to explain most of the experimental observations. Another minor consideration is that SAP iv produces stresses relative to the centroid of the element rather than the nodes, therefore the results listed in Table 5 are not exactly for locations such as the crests and valleys, but for locations approximately 3 mm away in the transverse direction. Hence these results obtained in the analysis of roofing without the washers cannot be directly compared with the corresponding results from ABAQUS as the latter results are for exact crests and valleys based on nodal stress results output from ABAQUS.

4.3 Roofing Fastened at Every Crest

4.3.1 Experimental results

The load-deflection curves at midspan for this series of tests are presented in Figure 19. The upward deflection of the valleys at midspan at any load level until failure was only slightly greater than that of the crests at the same cross-section, and thus only the latter deflections are plotted in Figure 19. The cross-sectional distortion observed in the previous series of tests did not occur as every corrugation was fastened. There was hardly any deflection at the central support and thus no such local plastic deformations occurred prematurely around the fasteners. The response to the applied loading was stable until at a later stage when diamond-shaped dimples formed under the screw heads at all the central support crests. Subsequent to this yielding at the central support, collapse occurred when roofing at both midspans also began to yield forming global plastic mechanisms which are shown in Figure 20. This ultimate failure occurred at 1250, 800, 700 and 470 N/f for roofing of test spans 250, 500, 650 and 1000 mm, respectively. In a two-span continuous beam subjected to midspan line loads, the bending moment at the central support is 20% greater than that at its midspan, and thus one would expect the failure to occur first at the central support and later at the midspans when such a beam was tested. This was observed in all the tests in this series.

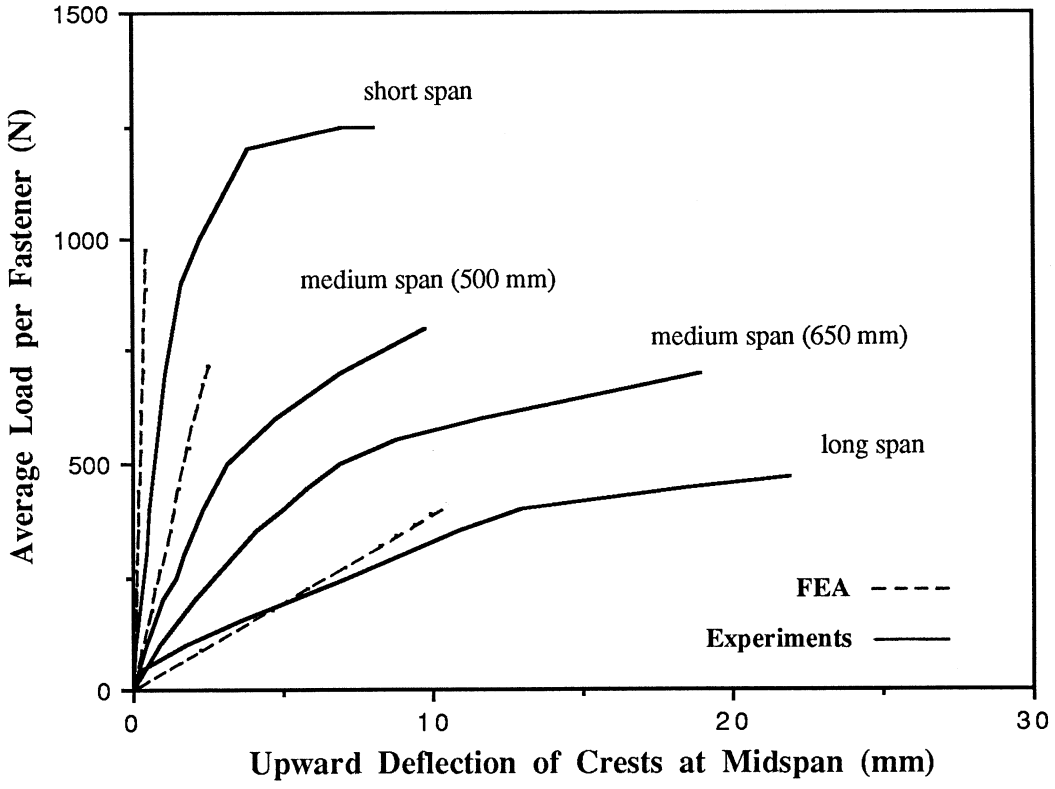

Figure 19. Load-deflection Curves for Corrugated Roofing Fastened at Every Crest

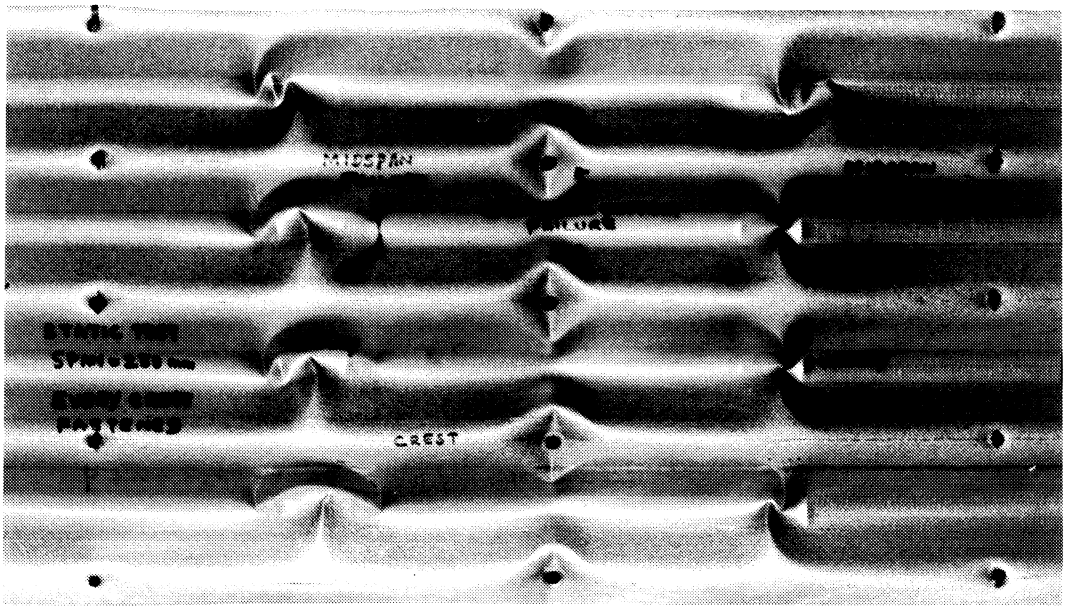

Figure 20. Ultimate Static Failure of Corrugated Roofing Fastened at Every Crest

4.3.2 Comparison of analytical and experimental results

The results from the FEA were obtained for the roofing of spans 250, 500 and 1000 mm until yielding commenced in the vicinity of the central support fasteners, and are compared with the corresponding experimental results in this section. A comparison between the experimental midspan crest deflections and those predicted by analysis is given in Figure 19. There is reasonable agreement between the two results. From the FEA, identical deflections were obtained for the crests and valleys at any cross-section along the span at any load level. Experiments indicate only a slight difference between the deflections of crests and valleys. The upward deflection of the valley next to the central support crest is negligible. These results confirm the absence of cross-sectional distortion.

The FEA indicates that transverse bending stresses and out-of-plane bending components in the longitudinal direction are quite insignificant in this case. The magnitude of maximum transverse bending stress at midspan is only about 15 MPa for the medium span roofing (500 mm), and is of the same order for all the spans of roofing at a load level of 250 N/f (compressive in the top surface and tensile in the bottom surface of roofing). This is only about 15% of the maximum midspan longitudinal bending stress in the medium span roofing, and is only about 5% of the maximum midspan transverse bending stress at an equivalent load level of 500 N/f for the same span of roofing fastened only at alternate crests (see Section 4.1.2). The magnitude of transverse bending stress in this case decreases further towards the central support. It is only 10 MPa at

the central support valley for the same span and load level mentioned earlier. However, large transverse and longitudinal bending stresses are present at the central support crests. The greatest transverse bending stress is at the points which are on the edge of the fastener hole and the line of central support.

Figures 21 (a) to (c) present the results of maximum longitudinal bending stresses at midspan and central support from the FEA and SET for roofing of short span, medium span (500 mm) and long span. Although stresses at midspan crests and central support valleys are tensile and those at midspan valleys are compressive, they are plotted using absolute values. The longitudinal bending stresses are mainly of membrane type along the span as the out-of-plane bending components are quite insignificant. Therefore, the difference between the top and bottom surface stresses is very small and in these figures, only the greater stress is plotted. Experimental results regarding stresses are not available for comparison with these analytical results. The SET stress results were obtained using the simple pure bending formula for the corresponding bending moments of a two-span continuous beam. The same value of second moment of area of the corrugated roofing calculated in Section 4.1.2 was used in these stress calculations. Except at the central support crests, the results from the FEA and SET are in good agreement. This is to be expected as cross-sectional distortion is absent in this case.

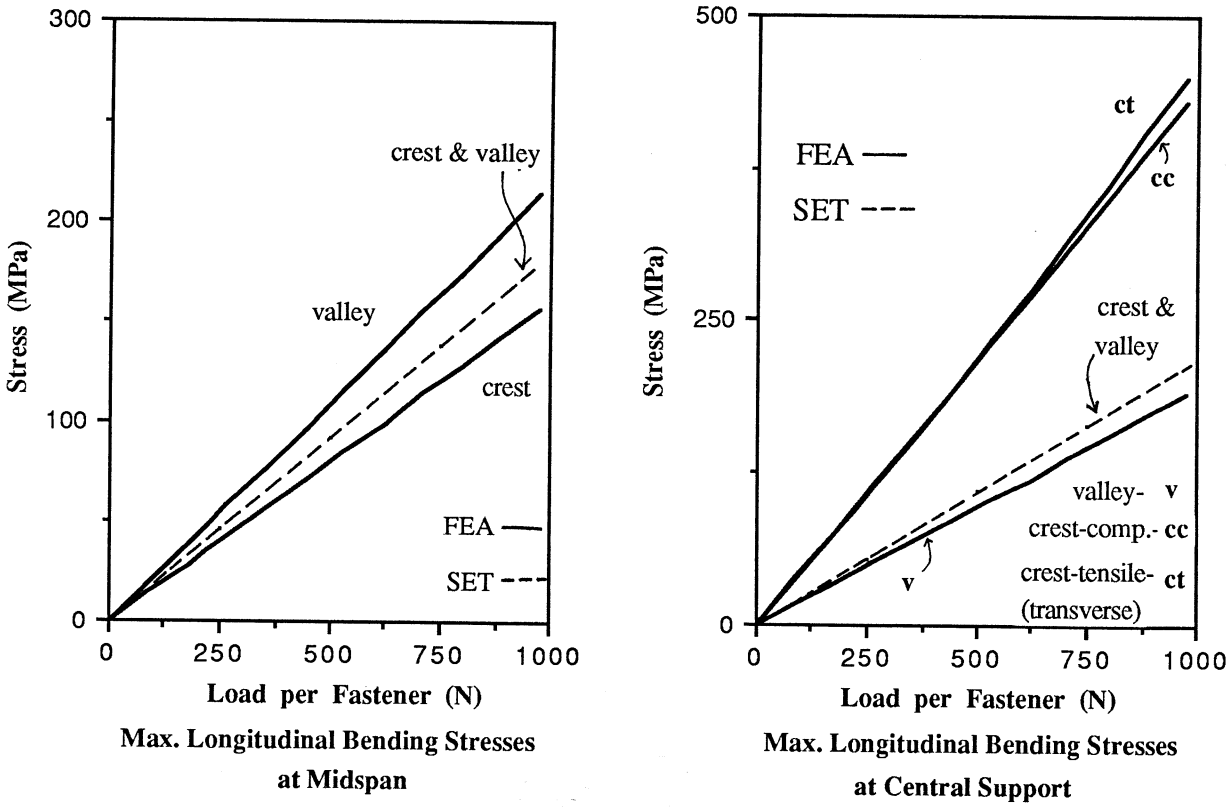

(a) Short Span Roofing

Figure 21. Stresses in Corrugated Roofing Fastened at Every Crest

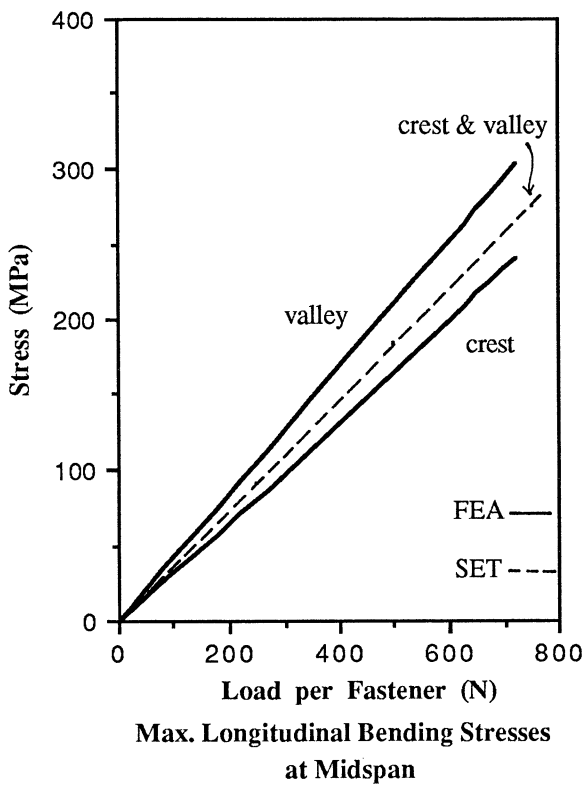

Max. Longitudinal Bending Stresses at Midspan

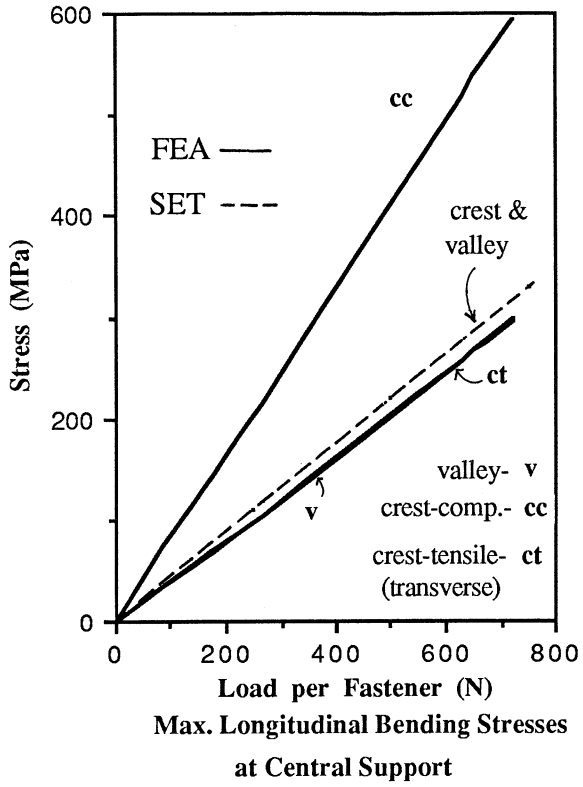

Max. Longitudinal Bending Stresses at Central Support

(b) Medium Span Roofing

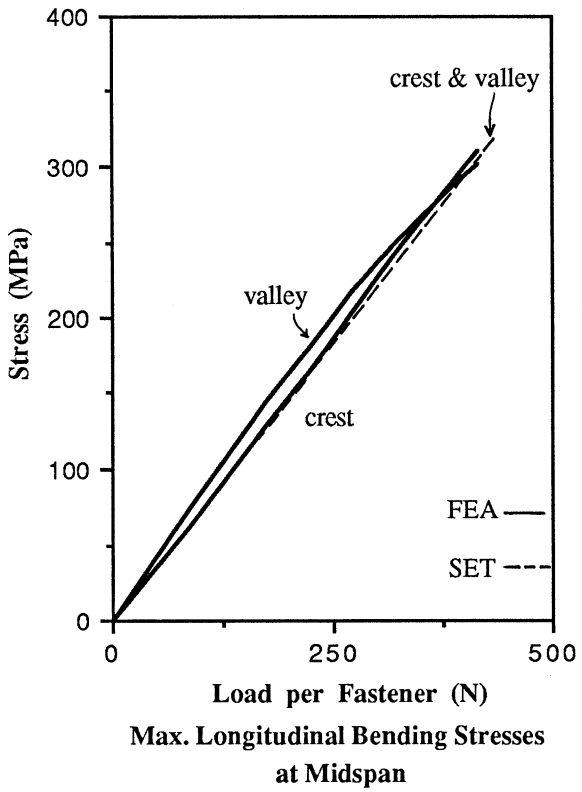

Max. Longitudinal Bending Stresses at Midspan

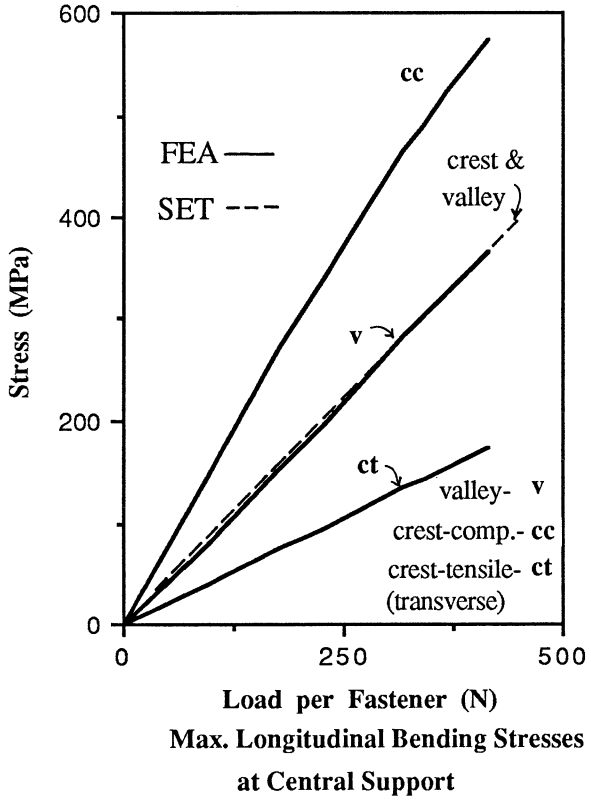

Max. Longitudinal Bending Stresses at Central Support

(c) Long Span Roofing

Figure 21. Stresses in Corrugated Roofing Fastened at Every Crest

As the maximum tensile stresses at the central support crest are in the transverse direction, they are also presented in Figure 21. The FEA reveals that there are larger stresses in the vicinity of the central support fasteners than anywhere else in the roofing. The maximum principal stress in the vicinity of the central support fasteners is of the same order as the maximum longitudinal bending stress given in Figure 21. Although the SET is able to predict the stresses along the spans, it is unable to predict the large ones in the vicinity of the fasteners.

4.4 Roofing Fastened at Alternate Valleys

4.4.1 Experimental results

In the absence of the knowledge gained from the investigation on roofing till now, one would expect only minor differences between the behaviour of roofing fastened at alternate valleys and that of roofing fastened at alternate crests. However, this series of tests on roofing fastened at alternate valleys revealed major differences between the two mentioned above. The load-deflection curves of the roofing of 650 mm test span can be considered to be typical of the load-deflection curves of all the spans in this case, and are shown in Figure 22.

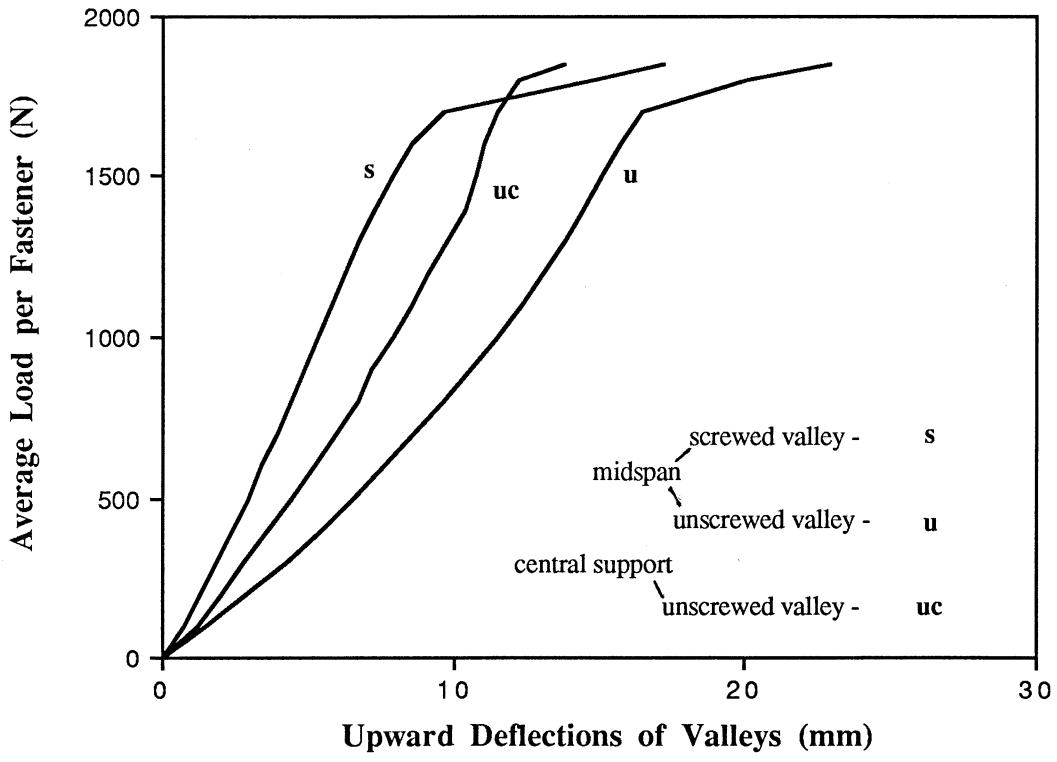

Figure 22. Load-deflection Curves for Corrugated Roofing Fastened at Alternate Valleys (test span = 650 mm)

During the initial stages of loading, the unscrewed valleys deflected many times greater than the adjoining screwed valleys at every cross-section. This effect was greater for shorter spans. These observations were similar to those made in the case of roofing fastened at alternate crests. The deflected mode caused significant cross-sectional distortion, especially at the central support as shown in Figure 23. However, the distortion was not as severe as that observed in the case of roofing fastened at alternate crests.

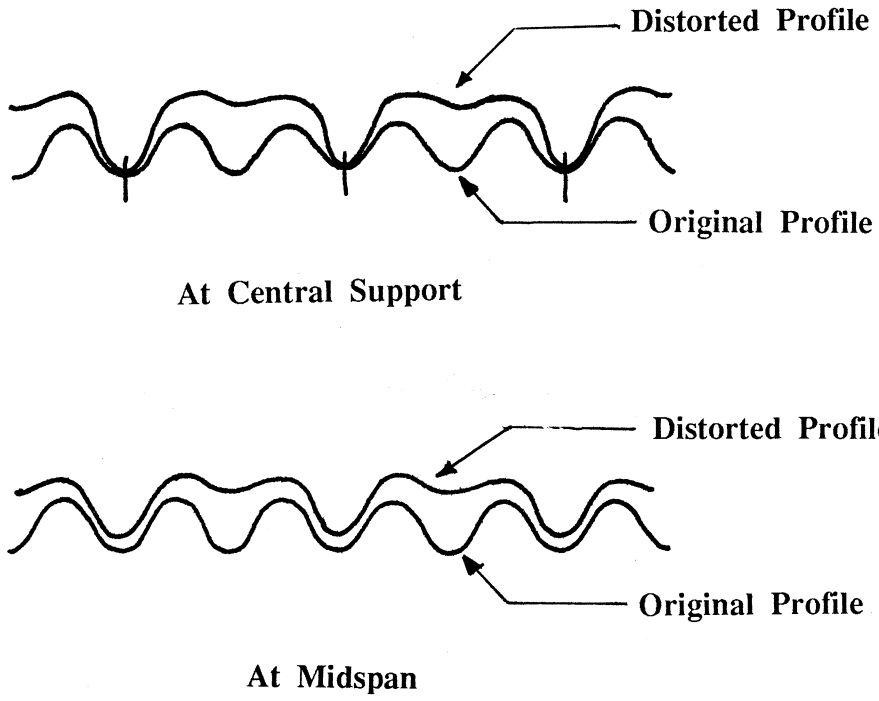

Figure 23. Cross-sectional Distortion of Corrugated Roofing Fastened at Alternate Valleys

The observations during the initial stages indicated similar behaviour to that of roofing fastened at alternate crests. However, in this series of tests on valley fastening the local plastic failure associated with buckling did not occur for any of the spans. By referring to Figure 23, the reason for the absence of local buckling under the screw heads can be understood. Unlike in the case of crest fastening where the mode of deformation is conducive to local buckling under the screw heads, the deformation mode in this case will not permit such buckling.

After some significant deformations and the resulting deeper cross-section, the roofing appeared to become stiffer as seen from the load-deflection graphs in Figure 22. This behaviour continued until the crests and valleys of each midspan cross-section began to deform severely and global plastic mechanisms formed at each midspan when valleys failed by buckling. Soon after this, a fracture occurred in the transverse

direction at each of the screwed valleys of the central support and in some cases the central support crests also failed by buckling. In the case of short span roofing, one of the central support fasteners pulled through the roofing before any global mechanism formed. This ultimate failure occurred at 1850, 2300 and 3000 N/f for roofing of medium spans (650 and 500 mm) and short span, respectively. Figure 24 shows a typical failed specimen with its global plastic mechanisms and the fracture at the central support.

Figure 24. Ultimate Static Failure of Corrugated Roofing Fastened at Alternate Valleys

In summary, it could be said that the major change in the behaviour of roofing when fastened at alternate valleys instead of alternate crests was the absence of stage 2 loading mentioned in Section 4.1.1. Due to this, the upward deflections were considerably less in the case of valley fastening despite the fact that both still had similar loading stages 1, 3 and 4.

4.4.2 Comparison of analytical and experimental results

As local plastic buckling did not occur in this case, the FEA was continued to a load level closer to the ultimate static failure load. But the analysis was conducted only for roofing of 500 mm span. Hence analytical and experimental results are compared only for this span of roofing as shown in Figure 25 (a). For other spans, only the experimental results are presented (Figures 22, 25 (b)). The overall agreement between the two results in Figure 25 (a) can be considered to be reasonably good. The FEA confirms all the general experimental observations made earlier regarding the initial cross-sectional distortion and the resulting stiffening during later stages of loading.

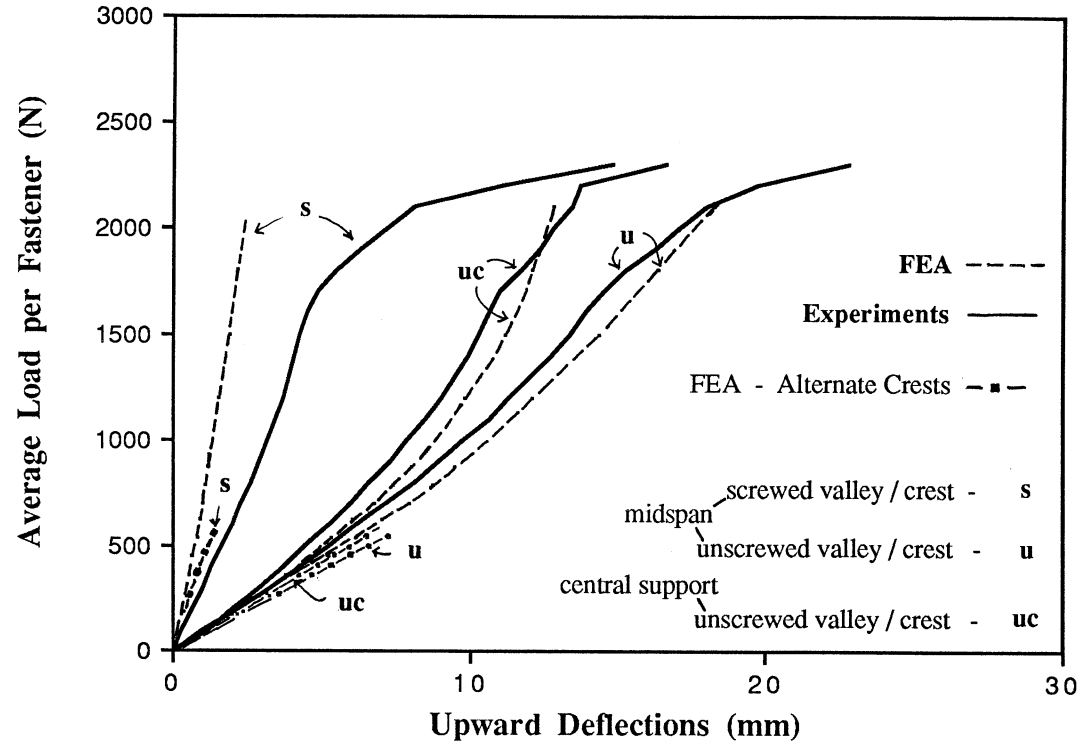

(a) Medium Span Roofing (test span = 500 mm)

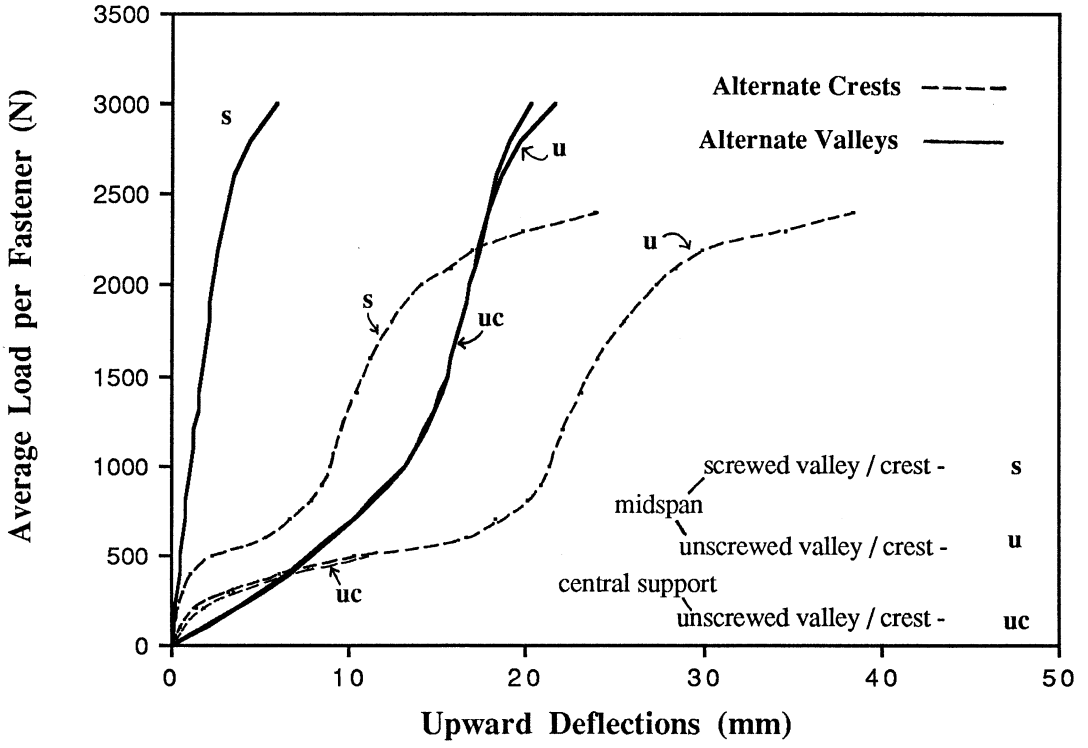

(b) Short Span Roofing (test span = 250 mm)

Figure 25. Load-deflection Curves for Corrugated Roofing Fastened at Alternate valleys

The analytical deflections during stage 1 loading for the roofing of 500 mm span fastened at alternate crests are also included in Figure 25 (a) for comparison with the corresponding results for valley fastening. It is clear that the deflections are less when valleys are fastened. It is to be noted that during the FEA of these two cases the same data file with only a single change of direction of loading (see Section 3.2) was used. However, it is interesting to note that they behave differently to each other. In Figure 25 (b), the entire experimental results for the roofing of 250 mm test span fastened at alternate crests are also included and they illustrate further the above mentioned observation. The absence of local plastic buckling in the case of valley fastening appears to have reduced the deflections considerably at a load level greater than 600 N/f.

The stress results from the FEA for the 500 mm span roofing show that large transverse bending stresses are present at the screwed valleys due to the cross-sectional distortion during initial stages of loading. However, this distortion is not so severe as in the case of roofing fastened at alternate crests and thus these stresses are below yield values until a load level of 1000 N/f. Beyond this, although the transverse bending stresses at some locations, mainly in the vicinity of the central support fastener holes are at yield values, it does not lead to the ultimate static failure. When the analytical load is closer to the experimentally observed ultimate failure load, the longitudinal bending stresses at the midspan valleys (compressive) and crests (tensile) and also at the central support valleys (tensile) are approaching yield values. These results explain the experimental observation of the formation of global plastic mechanisms at midspan involving valley buckling, followed by fracturing at central support valleys.

A summary of experimental results for corrugated roofing under midspan line loading are presented in Table 6.

Table 6. Summary of Experimental Results for Corrugated Roofing

Test Span (mm)	Equiv. Prototype End Span (mm)	Alt. Crests LPD Load (N/f)	Alt. Crests Ultimate Load (N/f)	Alt. Crests Cyclone Washers LPD Load (N/f)	Alt. Crests Cyclone Washers Ultimate Load (N/f)	Every Crest Ultimate Load (N/f)	Alt. Valleys Ultimate Load (N/f)
250	350	600	2400	1300	2400	1250	3000
500	700	625	2000	1000	2000	800	2300
650	900	650	1600	900	1600	700	1850
1000	1400	550	1100	750	1100	470	-

4.5 **Roofing Tested under Uniform Pressure Loading**

In the non-cyclonic areas, crest-fastening with three fasteners per sheet is recommended (LBI, 1987). This is in fact fastening every third or fourth crest as shown in Figure 26. The testing machine used in all the previous tests was not used in this case as the available space was insufficient to accommodate the width of roofing consisting of at least three fasteners. Hence an alternative testing method using air bags (Reardon, 1988) was used. This method illustrated in Figure 27 simulates uniform uplift pressure loading on roofing. Loading was applied by inflating the air bags and the test was controlled by the reaction measured at the central support.

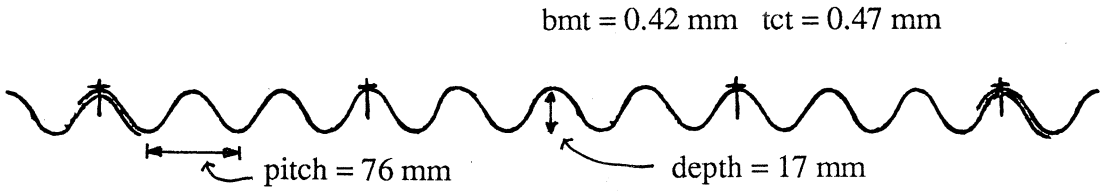

Figure 26. Corrugated Roofing Crest-fastened with Three Fasteners per Sheet

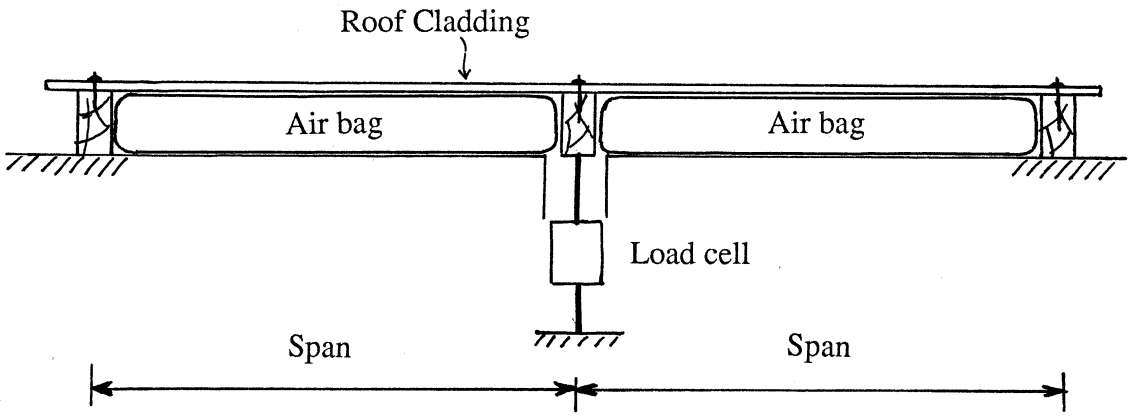

Figure 27. Test of Roofing under Uniform Pressure Loading

A full sheet with side laps was used to give a specimen width of 910 mm. A total of four fasteners of the type shown in Figure 2 (a) were used. For this specimen, the load in each of the central fasteners at the central support was estimated at 29% of the total central support reaction. Two tests were conducted on the same corrugated roofing used in the previous tests, but with different spans of 500 and 900 mm. These spans are equivalent to spans of 360 and 650 mm, respectively, if the previous testing method of midspan line loading is used. No analytical results are available for comparison in this case.

The overall behaviour observed during the current series of tests was similar to that of roofing fastened at alternate crests (Section 4.1.1). During the initial stage of loading, unscrewed crests and valleys deflected very severely causing large cross-sectional distortion. This stage was similar to the stage 1 loading observed in the tests on roofing fastened at alternate crests, but much greater deflections occurred in this case. Following this, the local plastic failure associated with buckling occurred at the central support fasteners at 600 and 400 N/f for 500 and 900 mm spans, respectively. The response to loading was again steady and resulted in a long stage 3 loading. In the present test set-up with uniform pressure loading, the midspan bending moment would have been quite small compared to that in the previous test set-up. Hence the ultimate failure occurred when one of the central support fastener pulled through the roof sheeting before the midspans could develop any global plastic mechanism. The ultimate failure loads were 2850 and 2350 N/f for the 500 and 900 mm spans, respectively.

A test on roofing fastened at alternate crests was also conducted under uniform pressure loading as it would verify the results obtained earlier using midspan line loading method. A wider test specimen (1520 mm) made by lapping a half sheet on either side of a full sheet was used. The specimen of 1200 mm span (equivalent to 870 mm if midspan line loading method is used) was held by ten fasteners. The central support reaction was assumed to be divided equally between fasteners. It was interesting to observe that the first local buckles appeared at 600 N/f. Because of the large number of fasteners, the load fluctuated during this stage and the last buckle formed at 670 N/f, beyond which the response to loading was steady again as in the tests conducted with midspan line loading. The ultimate failure occurred at 1450 N/f when a central support fastener pulled through the roofing. All these experimental results compare well with those obtained earlier from the tests with midspan line loading.

4.6 **Other Roofing Profiles**

A ribbed decking profile of dimensions shown in Figure 28 was tested using the same test set-up shown in Figure 27. Two tests were conducted with spans of 500 and 900 mm. A specimen of 800 mm width was fastened with five longer fasteners (65 mm), but of the same type used earlier in other tests. It was estimated that each of the three internal fasteners at the central support carried 25% of the total central support reaction. Figure 29 shows the typical load-deflection graphs in this case (that of 500 mm span). Analytical results are not available for this profile.

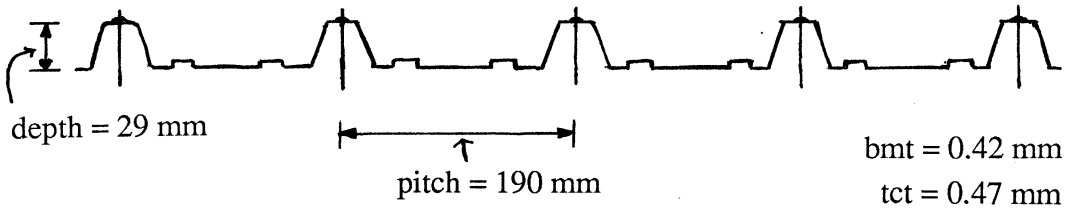

Figure 28. Dimensions of Decking Profile

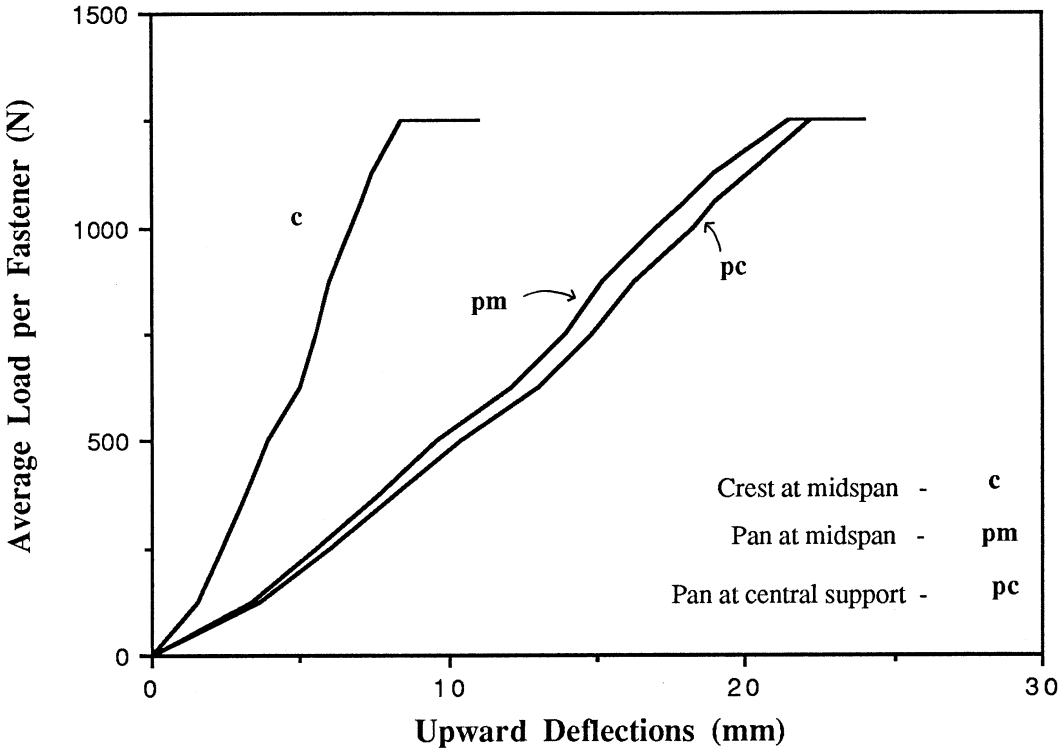

Figure 29. Load-deflection Curves for Ribbed Roof Decking

As the pan of this profile is quite wide, large cross-sectional distortion was observed due to the greater deflections of pans compared with that of the crests at every cross-section. At approximately 700 N/f, dimples formed under the internal fastener heads at the central support. Soon it appeared that localized yielding was occurring under the screw head. Unlike the crests of corrugated roofing, the crests of this trapezoidal profile are flat and wider. There was no sympathetic deformation of the sides of the crest to match the dimple formation. It could be said that yielding in this case was more localized than in the case of corrugated roofing. Hence, local plastic buckling did not occur for this decking profile. The small area of localized yielding under the screw heads did not affect the overall load-deflection behaviour of roofing as seen in Figure 29 in which the graphs are almost linear until the ultimate failure load. The ultimate failure occurred when one of the internal fasteners at the central support pulled through the crest of roofing at 1250 and 1300 N/f, for 500 and 900 mm spans, respectively. It is to be noted that the ultimate failure loads are almost the same for both spans of roofing because of the mode of failure.

From the limited number of tests in this case, it appears that large stresses could be present in the vicinity of fastener holes at rather smaller loads despite the absence of local plastic buckling. Therefore cracking may occur at the fastener hole under fatigue loading.

5. CORRELATION OF STATIC AND FATIGUE TEST RESULTS OF CORRUGATED ROOFING AND RELATED DISCUSSIONS

5.1 Roofing Fastened at Alternate Crests

Section 5 contains only limited discussions since all the fatigue test results are not yet available. The fatigue test results obtained to date are very much in accordance with the results from static analyses.

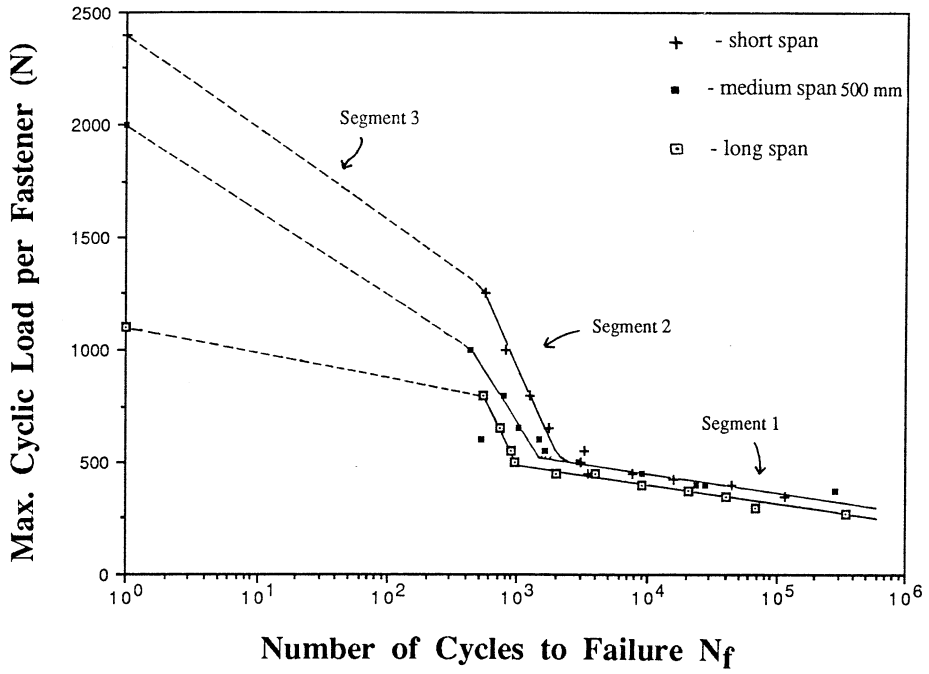

Figure 30. Fatigue Curves for Corrugated Roofing Fastened at Alternate Crests (cycling from zero minimum load)

As anticipated, low cycle fatigue cracking occurred for the roofing fastened at alternate crests. The fatigue curves obtained in this case consist of three linear segments due to the LPD load (Figure 30). Segment 1, for which the maximum cyclic load is less than the LPD load, corresponds to the stage 1 loading of static tests. The close proximity of the fatigue curves of segment 1 show that the stress levels in the vicinity of the central support fasteners causing fatigue cracks are approximately of the same order for all the spans. This was predicted by the static analyses. The greater cross-sectional distortion that occurs for shorter span roofing causes the overall stress levels in the vicinity of central

support fasteners to be of the same order for all the spans. These results are quite important as they mean that load per fastener is the most important parameter controlling the fatigue behaviour of such roofing assemblies. Hence they confirm the current design practice in which the fatigue test results for a single span of roofing are extrapolated to other spans. However, beyond the LPD load, as with the static load-deflection curves, the fatigue curves are not the same for all the spans. This means that both load per fastener and bending moment at the central support are important fatigue parameters above the LPD load, but this deduction may not be so important as the design load could never be greater than the LPD load.

It is pointed out that for all the spans of roofing, large stresses exist in the vicinity of the central support fasteners and local yielding occurs around the fasteners at the LPD load. The presence of reserve static strength beyond the LPD load is of no importance from a fatigue point of view. The cracks are likely to develop due to the high stress levels in the vicinity of the fasteners. This explains the commonly observed low cycle fatigue cracking of corrugated roofing.

The low cycle fatigue cracking that occurs prematurely in this case could be considered to be due to the local plastic buckling behaviour at comparatively smaller loads and as such the LPD load is an important parameter governing the fatigue behaviour of roofing fastened at alternate crests. Based on all the static test results available, the LPD load can be assumed to be 600 N/f for all of the most common spans. As anticipated from the static tests and confirmed by fatigue tests, the fatigue resistance is reduced by an order of magnitude when the applied load is greater than the LPD load. Hence the LPD load can be considered to be the ultimate load from a fatigue strength consideration although the corresponding ultimate static load is many times greater than the LPD load. However, it is interesting to note that the current design load used by the manufacturers of corrugated roofing is 550 N/f (LBI, 1987) which was determined based on results of fatigue tests to TR440 requirements (EBS, 1978). Although all the tests in this investigation indicated very little variation in the LPD load, the lower bound of the LPD load in a realistic situation could be less than that observed during these laboratory tests.

Considering the foregoing discussions, the current design load appears to be too close to the LPD load. Hence it may be appropriate to either reduce the current design load or to increase the LPD load of corrugated roofing. Obviously the building industry would prefer the latter approach and the use of cyclone washers can just do that. However, as the use of such washers is not so popular among the builders, one should investigate the possibility of increasing the LPD load by other means.

The LPD load is dependent on the geometry of the corrugated profile and the material properties. As the strength of the roofing material used at present is already high at the expense of loss of ductility, any attempt to increase the strength of the material further to achieve a greater LPD load may not be prudent. However, an attempt to determine the optimum geometry that would give the greatest LPD load is worthwhile, keeping in mind that major changes cannot be made to alter the overall appearance of the corrugated profile. To the author's knowledge, no analytical program is available that can be used to determine the LPD load and thus this investigation may have to be based on experiments alone. However, a lower bound load based on the first yield point in the vicinity of the central support fasteners can be determined for each geometry of the profile chosen using a finite element program like ABAQUS. This task of achieving the greatest LPD load for the corrugated roofing profile may appear to be tedious, but if completed would give some useful results to the building industry.

The other parameter that could affect the LPD load is the ductility of the roofing material. As explained earlier in Section 4.1, yielding occurs first at a point in the vicinity of the fastener holes, but spreads rapidly to other points in the vicinity due to the absence of ductility of material currently used (see Section 2.6). Once sufficient yielding has developed around the fastener hole, the local plastic buckling occurs. Hence by using a ductile material for the same geometry, one could increase the LPD load as yielding would not spread rapidly in this instant. But it is not known by how much it will be increased. It is thought that the improvement in the LPD load through the use of a ductile roofing material may not produce similar improvement in the fatigue strength. This is because the ductility of the material can only delay the local plastic buckling, but yielding would have already commenced in the vicinity of the fastener holes.

The LPD load may also depend on the shape and size of the fastener head and the neoprene washer underneath, and on the size of fastener hole. Despite lack of analytical and experimental evidence about this, one could say that these geometrical parameters cannot cause a significant improvement in the LPD load unless they are changed drastically, for example, the fastener head and neoprene washer have to be modified to be somewhat equivalent to cyclone washers.

5.2 **Roofing Fastened at Alternate Crests with Cyclone Washers**

A limited number of fatigue tests on roofing in this case revealed that the fatigue performance was significantly improved. This can be easily explained by the static analytical results which clearly showed that the

stress levels under the fastener heads at the central support are very much reduced when washers are used. It is to be noted that the LPD load is increased in this case for all the spans. For shorter spans, a greater design load per fastener may be used as the LPD load is significantly increased for these spans. During the fatigue tests, the usual cracks did not appear at the fastener holes, but tearing of roofing below the edge of the washer occurred which must have been due to the high stresses at these locations as indicated by the static analysis. However, it still did not let the screw pull through the roofing and thus no disengagement of roofing occurred. Hence it can be concluded that the use of cyclone washers in fastening the corrugated roofing at alternate crests is an effective method to prevent the premature cracking under the fastener heads and the resulting disengagement of roofing.

5.3 Roofing Fastened at Every Crest

In the case of fastening every crest of corrugated roofing, the fatigue curves (Figure 31) are smooth continuous curves which is in accordance with the static load-deflection curves. There was no anomalous behaviour here, but cracking still occurred under the fastener heads. This can be explained by the presence of larger stresses at the fastener hole. The results indicate that both load per fastener and bending moment at the support are important parameters governing the fatigue behaviour when every crest is fastened.

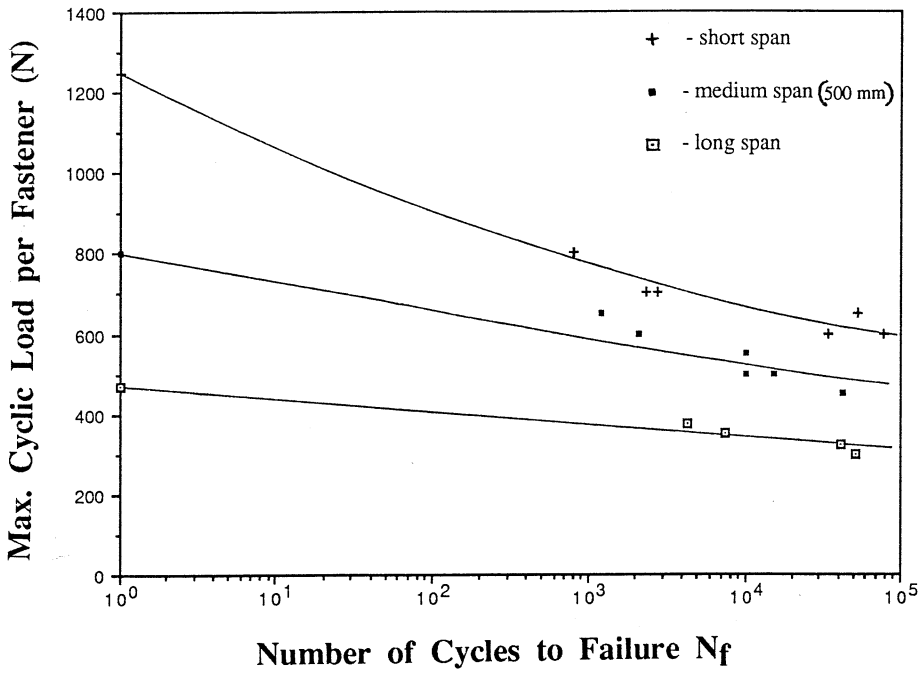

Figure 31. Fatigue Curves for Corrugated Roofing Fastened at Every Crest (cycling from zero minimum load)

5.4 Roofing Fastened at Alternate Valleys

No fatigue test results are available for valley fastening, but from the static analysis, it is anticipated that fatigue performance will be improved due to the absence of premature local plastic deformations at the central support.

6. CONCLUSIONS

The following conclusions have been drawn from this investigation on corrugated roofing to date.

(1) The behaviour of corrugated roofing subjected to uplift wind loads was dependent on the type of fastening system used.

(2) The results from a finite element analysis agreed reasonably well with experimental results in all cases of corrugated roofing of different spans (test spans of 250, 500, 650 and 1000 mm - equivalent prototype end spans of 350, 700, 900 and 1400 mm) and fastening systems. However, the results from simple engineering calculations did not agree with experimental results except in the case of roofing fastened at every crest.

(3) For alternate crest fastening which is the most common system in cyclone prone areas, large cross-sectional distortion took place leading to an initial local plastic failure at approximately the same load per fastener for all the spans (LPD load - 550 to 650 N/f). The initial failure was localized to a smaller region around the central support fasteners, and there was reserve static strength beyond the initial failure, particularly for shorter spans of roofing. However, when the roofing was fastened at every crest or alternate valleys, the behaviour was totally different with no such complicated loading paths via the LPD load.

(4) The static results revealed the presence of large stresses in the vicinity of the central support fasteners and yielding at the LPD load for all the spans of roofing fastened at alternate crests. This explains the low cycle fatigue cracking at these locations. The reserve static strength beyond the LPD load is of no importance from a fatigue point of view and the LPD load should be considered the ultimate fatigue load.

(5) The use of cyclone washers at alternate crests restricted the cross-sectional distortion that occurred otherwise and thus delayed the

initial local plastic failure for all the spans. The LPD load was significantly increased, especially for shorter spans of roofing. The region below the fastener heads was free of large stresses and thus no premature cracking could occur at these locations. Despite some tearing which could occur in the roofing under the longitudinal edge of the washer, the use of washers is an effective method in preventing premature fatigue cracking and resulting disengagement of roofing.

(6) It is clear that fatigue performance of roofing fastened at alternate crests can be improved if the LPD load is raised. If cyclone washers are not used for this purpose, attempts should be made to optimise the geometry of the corrugated profile that gives the greatest LPD load.

(7) When every crest was fastened, no cross-sectional distortion occurred prematurely and the behaviour was not complicated. The roofing in this case behaved almost like an ideal two-span continuous beam and as such its behaviour was predictable even by simple engineering calculations.

(8) When alternate valleys were fastened, cross-sectional distortion occurred during initial stages, but not as severe as in the case when alternate crests were fastened. The distortion led to an overall stiffening with no local plastic failure. The static results indicated that fatigue performance could be improved in this case, but no fatigue test results are yet available to confirm this.

(9) The fatigue performance of corrugated roofing with different spans and fastening systems was explained satisfactorily using the static results.

(10) For corrugated roofing fastened at alternate crests without cyclone washers, the load per fastener was the only critical parameter controlling its fatigue behaviour, but when fastened in other ways such as every crest fastening, both load per fastener and bending moment at the central support were critical.

7. ACKNOWLEDGEMENTS

The author wishes to thank
(1) Lysaght Building Industries for donating the corrugated roof sheeting to the Cyclone Testing Station's specifications,
(2) W.A. Deutsher Pty. Ltd. for donating the fasteners,

(3) the Station's Technical Director, Mr G.F. Reardon and Professor G.R. Walker of the Dept. of Civil and Systems Engineering, James Cook University for their support and guidance in this research project,
(4) Dr B.S. Best of the Dept. of Civil and Systems Engineering, James Cook University for his help in the use of finite element program SAP iv,
(5) the Station's technical staff, Messrs. W. Morris and K. Abercombie for their technical assistance, and
(6) Monash University for providing computing facilities.

Special thanks to Mr Reardon for his help in the preparation of this report.

8. REFERENCES

Bathe, K.J., Wilson, E.L. and Peterson, F.E. (1974) SAP iv - A Structural Analysis Program for Static and Dynamic Response of Linear Systems, University of California, Berkeley, California, USA.

Beck, V.R. (1978) Wind Loading Failures of Corrugated Roof Cladding, M.Eng.Sc. Thesis, Dept. of Civil Engineering, University of Melbourne.

Beck, V.R. and Morgan, J.W. (1975) Appraisal of Metal Roofing under Repeated Wind Loading - Cyclone Tracy Darwin 1974, Australian Dept. of Housing and Construction, Housing Research Branch, Technical Report No.1, February.

Beck, V.R. and Stevens, L.K. (1979) Wind Loading Failures of Corrugated Roof Cladding, Civil Engineering Transactions, Institution of Engineers, Australia, Vol. CE 21, No.1, pp. 45-56.

Darwin Reconstruction Commission (DRC) (1976), DABM - Darwin Area Building Manual, Darwin.

Experimental Building Station (EBS) (1978) TR440 - Guidelines for the Testing and Evaluation of Products for Cyclone prone areas, Sydney.

Hibbitt, Karlsson and Sorensen (1984), ABAQUS User's Manual, USA.

Lysaght Building Industries (1987), LBI Reference Manual.

Morgan, J.W. and Beck, V.R. (1977) Failure of Sheet-metal Roofing under Repeated Wind Loading, Civil Engineering Transactions, Institution of Engineers, Australia, Vol. CE 19, No.1, pp.1-5.

Neal, T.P. (1984) The Structural Performance of Nail-fixed Corrugated Sheet Steel Roof Cladding, Technical Report, Building Research Association of New Zealand, Wellington, New Zealand.

Perry, J.H. and Perry, R.H. (1959) Engineering Manual, McGraw-Hill, New York, USA.

Reardon, G.F. (1980) Recommendations for the Testing of Roofs and Walls to Resist High Wind Forces, Technical Report No. 5, Cyclone Testing Station, James Cook University.

Reardon, G.F. (1988) Towards a Standard Test Method for Cycling Sheet Roofing, Paper presented to Workshop on Review of TR440 - Guidelines for the Testing and Evaluation of Products for Cyclone prone Areas, National Building Technology Centre, Sydney.

Reardon, G.F., Walker, G.R., and Jancauskas, E.D. (1986) Effects of Cyclone Winifred on Buildings, Technical Report No. 28, Cyclone Testing Station, James Cook University.

Salaheldin, M., Schmidt, L.C. and Upfold, R.W. (1987) Deflection Behaviour of Statically Loaded Corrugated Sheet, Proc. of the First National Structural Engineering Conference, Melbourne, August, pp.541-545.

Slogrove, T. (1985) Investigation of Fatigue Failure of Steel Cladding under Wind Loads, B.Eng. Thesis, James Cook University, Australia.

Standards Association of Australia (SAA) (1974) AS 1391 - Methods for Tensile Testing of Metals.

Standards Association of Australia (SAA) (1984) AS 1397 - Steel Sheet and Strip - Hot-dipped Zinc-coated or Aluminium/Zinc-coated.

Standards Association of Australia (SAA) (1977) AS 1445 - 76 mm pitch Corrugated Hot-dipped Zinc-coated or Aluminium/Zinc-coated Steel Sheet.

Standards Association of Australia (SAA) (1980) AS 1562 - Design and Installation of Metal Roofing.

Walker, G.R. (1975) Report on Cyclone Tracy - Effect on Buildings - December 1974, Vol. 1, Australian Dept. of Housing and Construction, Melbourne, March.

APPENDIX A

Bending Stresses in MPa for Corrugated Roofing Fastened at Alternate Crests

Table A1 (a). Midspan Longitudinal Bending Stresses - Short Span

Load/f (N)		Crests, Valleys SET	Unscrewed Crest FEA	Unscrewed Crest Expt.	Valley FEA	Valley Expt.	Screwed Crest FEA	Screwed Crest Expt.
200	T	20	55	23	-17	-19	-30	30
	B	20	-24	17	-29	-23	71	27
400	T	39	98	53	-29	-59	-59	83
	B	39	-34	41	-72	-68	155	75
500	T	49	116	67	-36	-76	-71	105
	B	49	-34	53	-100	-88	205	96
550	T	54	124	77	-39	-84	-76	118
	B	54	-32	62	-114	-95	229	108

Table A1 (b). Midspan Transverse Bending Stresses - Short Span

Load/f (N)		Crests, Valleys SET	Unscrewed Crest FEA	Unscrewed Crest Expt.	Valley FEA	Valley Expt.	Screwed Crest FEA	Screwed Crest Expt.
200	T	-	131	58	16	23	-170	-141
	B	-	-129	-65	-19	-15	173	138
400	T	-	219	162	65	60	-360	-327
	B	-	-214	-180	-70	-35	368	314
500	T	-	249	206	99	83	-465	-435
	B	-	-242	-230	-105	-51	475	418
550	T	-	260	229	116	98	-514	-505
	B	-	-252	-255	-123	-61	525	482

Notes for Tables A1 to A6 :

1. FEA = Finite Element Analysis
2. SET = Simple Engineering Theory
   (SET gives the same magnitude of longitudinal stresses for screwed and unscrewed crests, and valleys. It does not predict the transverse bending stresses in the roofing)
3. Expt. = Experiments on strain gauged roofing specimens
4. T, B = Top, Bottom surfaces of roofing
5. The stresses at screwed crest of the central support are given separately in Appendix B
6. Short span, Medium span and Long span refer to test spans of 250, 500 and 1000 mm, respectively.

Table A2. Midspan Bending Stresses - Medium Span (FEA results only)

Load/f (N)		Crests, Valleys SET Longl.	Unscrewed Crest Longl.	Unscrewed Crest Transv.	Valley Longl.	Valley Transv.	Screwed Crest Longl.	Screwed Crest Transv.
200	T	39	52	73	-41	0.3	13	-87
	B	39	7	-71	-45	-3	64	91
400	T	78	101	133	-82	10	30	-179
	B	78	18	-128	-95	-16	134	185
500	T	97	125	159	-104	19	42	-225
	B	97	27	-152	-123	-26	172	232
550	T	107	135	168	-113	24	49	-245
	B	107	31	-161	-136	-32	190	253

Table A3 (a). Midspan Longitudinal Bending Stresses - Long Span

Load/f (N)		Crests, Valleys SET	Unscrewed Crest FEA	Unscrewed Crest Expt.	Valley FEA	Valley Expt.	Screwed Crest FEA	Screwed Crest Expt.
200	T	78	80	77	-82	-68	63	66
	B	78	54	65	-85	-80	86	66
400	T	156	161	145	-160	-147	138	171
	B	156	117	127	-168	-163	177	161
500	T	194	199	182	-195	-194	180	234
	B	194	150	160	-206	-213	223	222
550	T	214	218	200	-212	-227	202	286
	B	214	166	174	-224	-244	247	270

Table A3 (b). Midspan Transverse Bending Stresses - Long Span

Load/f (N)		Crests, Valleys SET	Unscrewed Crest FEA	Unscrewed Crest Expt.	Valley FEA	Valley Expt.	Screwed Crest FEA	Screwed Crest Expt.
200	T	-	38	-30	-5	24	-44	-58
	B	-	-34	-2	0.6	20	47	23
400	T	-	63	-29	-6	53	-78	-133
	B	-	-56	-33	-2	43	84	49
500	T	-	70	-25	-6	66	-89	-181
	B	-	-61	-54	-4	57	97	67
550	T	-	72	-32	-6	76	-93	-208
	B	-	-62	-51	-6	64	101	69

Table A4. Central Support Bending Stresses - Short Span

Load/f (N)		LONGITUDINAL STRESSES					TRANSVERSE STRESSES			
		Crests, Valleys SET	Unscrewed Crest		Valley		Unscrewed Crest		Valley	
			FEA	Expt.	FEA	Expt.	FEA	Expt.	FEA	Expt.
200	T	23	31	-4	21	17	131	64	18	25
	B	23	-47	-3	14	14	-131	-67	-14	-10
400	T	47	48	5	58	40	220	161	74	50
	B	47	-83	3	20	25	-220	-174	-68	-25
500	T	58	52	6	84	55	251	210	115	70
	B	58	-97	2	22	30	-251	-224	-110	-40
550	T	64	53	6	98	65	262	229	137	82
	B	64	-103	2	22	35	-262	-246	-133	-55

Table A5. Central Support Bending Stresses - Medium Span (FEA results only)

Load/f (N)		Crests, Valleys SET Longl.	Unscrewed Crest		Valley	
			Longl.	Transv.	Longl.	Transv.
200	T	47	-9	75	38	4
	B	47	-52	-75	40	-2
400	T	93	-21	141	85	24
	B	93	-103	-142	79	-20
500	T	117	-29	170	114	40
	B	117	-128	-171	99	-36
550	T	128	-33	182	128	49
	B	128	-139	-183	108	-45

Table A6. Central Support Bending Stresses - Long Span

Load/f (N)		LONGITUDINAL STRESSES					TRANSVERSE STRESSES			
		Crests, Valleys SET	Unscrewed Crest		Valley		Unscrewed Crest		Valley	
			FEA	Expt.	FEA	Expt.	FEA	Expt.	FEA	Expt.
200	T	93	-65	-50	82	62	46	56	3	28
	B	93	-90	-47	86	73	-48	-39	-1	24
400	T	187	-129	-114	177	162	98	150	16	69
	B	187	-182	-108	178	182	-101	-111	-12	75
500	T	234	-158	-156	228	227	122	220	29	98
	B	234	-225	-149	225	264	-126	-162	-24	96
550	T	257	-173	-199	255	292	134	284	37	127
	B	257	-246	-189	248	291	-137	-213	-32	122

APPENDIX B

Table B1. Stresses in the Vicinity of Central Support Fasteners (MPa) for Short Span Roofing Fastened at Alternate Crests

Load/f (N)		Node 14 Longl. FEA	Node 14 Transv. FEA	Node 14 Transv. FEA	Node 12 Longl. FEA	Node 12 Longl. Expt.	Node 12 Transv. FEA	Node 12 Transv. Expt.	Node 12 Transv. FEA	Node 42 Longl. FEA	Node 42 Transv. FEA	Node 42 Transv. FEA
200	T	-246	-610		-109	46	-255	-26		-92	-84	
	B	128	559		38	-23	134	7		-9	55	
	PT	-231	-625	(547)	-108	46	-256	-26	(223)	-116	-60	(101)
	PB	121	566	(516)	19	-23	152	7	(144)	-9	55	(60)
400	T	-391	-780		-231	108	-508	-43		-229	-200	
	B	265	772		74	-32	267	-13		-10	125	
	PT	-376	-796	(690)	-226	108	-513	-43	(445)	-290	-139	(251)
	PB	256	781	(690)	36	-33	305	-12	(288)	-12	127	(133)
500	T	-425	-783		-276	155	-553	9		-304	-247	
	B	313	782		83	-58	307	-100		-6	153	
	PT	-412	-797	(690)	-264	155	-566	9	(490)	-372	-179	(322)
	PB	305	790	(690)	32	-57	358	-101	(343)	-9	155	(160)
550	T	-434	-782		-294	183	-567	61		-328	-245	
	B	326	785		85	-70	321	-178		-3	172	
	PT	-419	-796	(690)	-278	183	-584	61	(506)	-389	-184	(337)
	PB	319	792	(690)	27	-69	378	-179	(366)	-7	176	(179)

Load/f (N)		Node 40 Longl. FEA	Node 40 Transv. FEA	Node 40 Transv. FEA	Node 47 Longl. FEA	Node 47 Transv. FEA	Node 47 Transv. FEA	Node 49 Longl. FEA	Node 49 Longl. Expt.	Node 49 Transv. FEA	Node 49 Transv. Expt.	Node 49 Transv. FEA
200	T	-118	-252		67	39		-77	7	-90	-244	
	B	36	278		-114	-37		14	-17	149	217	
	PT	-116	-253	(220)	70	35	(61)	-53	8	-113	-245	(98)
	PB	34	280	(264)	-130	-22	(121)	-4	-17	167	217	(169)
400	T	-251	-512		97	61		-170	40	-209	-560	
	B	73	553		-239	-81		18	-31	317	490	
	PT	-247	-515	(447)	103	55	(89)	-119	42	-259	-562	(224)
	PB	68	558	(527)	-269	-50	(248)	-18	-32	352	491	(362)
500	T	-299	-558		73	52		-230	75	-294	-690	
	B	96	599		-306	-113		11	-83	408	690	
	PT	-296	-560	(485)	80	45	(69)	-165	76	-359	-690	(311)
	PB	92	602	(562)	-345	-74	(315)	-34	-87	453	690	(471)
550	T	-317	-575		53	46		-257	125	-332	-690	
	B	104	607		-335	-126		5	-143	447	690	
	PT	-315	-577	(501)	60	36	(54)	-185	140	-405	-690	(351)
	PB	101	610	(567)	-378	-84	(343)	-43	-170	495	690	(518)

Table B2. Stresses in the Vicinity of Central Support Fasteners (MPa) for Medium Span Roofing Fastened at Alternate Crests FEA Results Only

Load/f (N)	Node 14 Longl.	Transv.		Node 12 Longl.	Transv.		Node 42 Longl.	Transv.	
200 T	-176	-373		-92	-138		-111	-68	
B	47	322		-13	54		-41	32	
PT	-165	-385	(334)	-90	-140	(123)	-127	-52	(111)
PB	43	325	(307)	-23	64	(78)	-41	32	(63)
400 T	-367	-764		-196	-295		-239	-144	
B	102	689		-25	123		-86	68	
PT	-341	-789	(685)	-193	-298	(262)	-273	-111	(238)
PB	93	675	(657)	-44	142	(168)	-86	68	(134)
500 T	-410	-774		-252	-370		-318	-195	
B	157	744		-34	152		-107	94	
PT	-388	-797	(690)	-247	-376	(331)	-366	-148	(319)
PB	148	752	(690)	-59	178	(214)	-107	94	(174)
550 T	-424	-775		-279	-405		-357	-220	
B	180	751		-38	166		-117	107	
PT	-403	-797	(690)	-272	-412	(363)	-411	-165	(359)
PB	171	760	(690)	-66	195	(235)	-117	107	(194)

Load/f (N)	Node 40 Longl.	Transv.		Node 47 Longl.	Transv.		Node 49 Longl.	Transv.	
200 T	-103	-144		-44	2		-94	-58	
B	-20	141		-115	-28		-41	79	
PT	-100	-146	(129)	-44	2	(45)	-102	-50	(88)
PB	-21	141	(153)	-119	-23	(110)	-46	84	(115)
400 T	-219	-309		-101	1		-200	-126	
B	-42	300		-242	-59		-89	169	
PT	-214	-314	(278)	-101	1	(101)	-218	-109	(189)
PB	-42	301	(324)	-252	-49	(231)	-99	180	(245)
500 T	-285	-404		-139	-3		-262	-169	
B	-54	388		-312	-78		-117	221	
PT	-278	-411	(363)	-139	-3	(137)	-286	-145	(248)
PB	-55	389	(419)	-325	-65	(298)	-130	234	(320)
550 T	-316	-450		-159	-6		-291	-190	
B	-60	429		-346	-87		-130	245	
PT	-309	-457	(404)	-159	-6	(156)	-319	-162	(276)
PB	-61	431	(464)	-360	-73	(330)	-145	260	(355)

Table B3. Stresses in the Vicinity of Central Support Fasteners (MPa) for Long Span Roofing Fastened at Alternate Crests

Load/f (N)		Node 14 Longl. FEA	Node 14 Transv. FEA	Node 14 Transv. FEA	Node 12 Longl. FEA	Node 12 Longl. Expt.	Node 12 Transv. FEA	Node 12 Transv. Expt.	Node 12 Transv. FEA	Node 42 Longl. FEA	Node 42 Transv. FEA	Node 42 Transv. FEA
200	T	-166	-249		-111	6	-84	40		-156	-56	
	B	-14	218		-63	-82	23	-54		-93	17	
	PT	-150	-264	(230)	-112	6	-83	40	(101)	-166	-46	(148)
	PB	-16	220	(228)	-66	-82	26	-54	(82)	93	18	(103)
400	T	-354	-557		-232	78	-193	145		-318	-119	
	B	-13	497		-116	-230	64	-204		-184	41	
	PT	-322	-589	(509)	-235	78	-190	145	(216)	-340	-97	(304)
	PB	-16	500	(511)	-123	-231	72	-203	(170)	-184	42	(209)
500	T	-455	-733		-294	227	-260	361		-401	-154	
	B	-3	660		-136	-354	93	-520		-227	56	
	PT	-415	-773	(669)	-302	226	-253	362	(280)	-431	-125	(384)
	PB	-8	665	(671)	-146	-353	104	-521	(217)	-228	57	(261)
550	T	-474	-758		-324	-	-293	-		-446	-176	
	B	24	693		-146	-	107	-		-246	67	
	PT	-436	-796	(690)	-335	-	-282	-	(312)	-480	-142	(427)
	PB	19	699	(690)	-158	-	118	-	(240)	-247	68	(286)

Load/f (N)		Node 40 Longl. FEA	Node 40 Transv. FEA	Node 40 Transv. FEA	Node 47 Longl. FEA	Node 47 Transv. FEA	Node 47 Transv. FEA	Node 49 Longl. FEA	Node 49 Longl. Expt.	Node 49 Transv. FEA	Node 49 Transv. Expt.	Node 49 Transv. FEA
200	T	-130	-100		-152	-22		-145	-71	-46	-117	
	B	-75	79		-161	-28		-107	-84	49	155	
	PT	-134	-97	(119)	-153	-22	(143)	-147	-71	-43	-117	(131)
	PB	-78	79	(133)	-162	-26	(151)	-108	-84	49	155	(140)
400	T	-269	-227		-294	-41		-288	-156	-103	-385	
	B	-141	187		-329	-60		-209	-232	114	475	
	PT	-280	-218	(254)	-295	-40	(278)	-302	-156	-97	-385	(267)
	PB	-141	187	(285)	-334	-55	(310)	-211	-232	116	475	(287)
500	T	-342	-304		-361	-49		-373	-210	-137	-651	
	B	-168	254		-415	-77		-257	-318	153	690	
	PT	-358	-288	(329)	-362	-48	(340)	-382	-205	-128	-656	(336)
	PB	-169	254	(368)	-421	-71	(391)	-260	-322	156	690	(363)
550	T	-379	-346		-393	-54		-412	-	-156	-	
	B	-181	291		-459	-86		-279	-	174	-	
	PT	-398	-326	(367)	-395	-52	(371)	-422	-	-146	-	(371)
	PB	-181	291	(412)	-466	-79	(432)	-283	-	178	-	(402)

Notes for Tables B1 to B3 :

1. FEA = Finite Element Analysis
2. Expt. = Experiments on strain gauged roofing specimens

3. T, B = Stresses on Top, Bottom surfaces of roofing
4. PT, PB = Principal Stresses on Top, Bottom surfaces of roofing

5. von Mises equivalent stress from FEA is given inside brackets

6. Short span, Medium span and Long span refer to test spans of 250, 500 and 1000 mm, respectively

7. The figure below shows the locations of nodes 14, 12, 42, 40, 47 and 49.

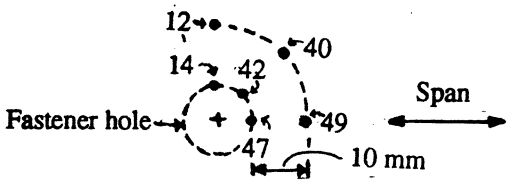

Location of Nodes